JOURNAL OF GUIDANCE, CONTROL, AND DYNAMICS
Vol. 32, No. 1, January–February 2009

Multicriteria Comparison Among Several Mitigation Strategies for Dangerous Near-Earth Objects

J. P. Sanchez,* C. Colombo,† M. Vasile,‡ and G. Radice§
University of Glasgow,
Glasgow, Scotland G12 8QQ, United Kingdom

DOI: 10.2514/1.36774

In this paper, a comparative assessment of the effectiveness of different deviation methods for near-Earth objects is presented. Specifically, a solar collector, nuclear interceptor, kinetic impactor, low-thrust propulsion, mass driver, and gravity tug are modeled and compared. For each method, a mathematical model is developed to compute the achievable deviation. A multicriteria optimization method is then used to construct the set of Pareto-optimal solutions, minimizing the mass of the spacecraft at departure from the Earth and the warning time (i.e., the time from launch to the foreseen impact of the asteroid with the Earth), while maximizing the deviation. A dominance criterion is defined and used to compare all of the Pareto sets for all of the various mitigation strategies. Finally, a technology readiness level factor is associated with each strategy to estimate the required technological development.

Nomenclature

A_m	=	cross-sectional area of the mirror, m^2
A_s	=	area of the illuminated spot, m^2
a	=	semimajor axis of an orbit, km
b	=	semiminor axis of an orbit, km
c	=	heat capacity, J/kg/K
d	=	hovering distance, m
E_A	=	received energy per unit area, J/m^2
E_t	=	total energy released by the nuclear interceptor, J
E_v	=	energy of sublimation, J/g
e	=	eccentricity of an orbit
$\mathrm{erfc}(f(x))$	=	complementary error function of $f(x)$
F_g	=	gravity attraction between the spacecraft and the asteroid, N
F_{hover}	=	effective vertical thrust, N
G	=	universal gravitational constant, 6.67259×10^{-11} $m^3/kg/s^2$
g_0	=	standard free-fall constant, 9.81 m/s^2
H	=	altitude of detonation of the nuclear interceptor, m
h	=	distance from the nuclear explosion to a specific point on the surface of the asteroid, m
I_{sp}	=	specific impulse of a propulsion system, s
i	=	inclination of an orbit, deg
k	=	Boltzmann constant, 1.380658×10^{-23} J/K
M	=	mean anomaly of an orbit, deg
M_a	=	mass of the asteroid, kg
M_m	=	molecular mass, kg
m_A	=	mass per unit area, kg/m^2
m_d	=	dry mass of the spacecraft, kg
m_{debris}	=	mass of the nuclear interceptor's debris that impacts the asteroid, kg
m_i	=	mass of the spacecraft at the near-Earth object arrival, kg
m_{launch}	=	mass expelled per shot by the Mass driver method, kg
m_{power}	=	mass of the power subsystem, kg
m_{wh}	=	mass of the nuclear warhead, kg
m_0	=	mass launched into space, kg
n	=	angular velocity of an orbit, s^{-1}
P_K	=	kinetic power provided by the mass driver, W
P_{in}	=	radiation power density over the illuminated surface of the asteroid, W/m^2
p	=	semilatus rectum of an orbit, km
p_A	=	linear momentum per unit area, kg/s/m
Q_{cond}	=	heat-flux loss by conduction, W/m^2
Q_{rad}	=	heat-flux loss by radiation, W/m^2
R_a	=	mean radius of the near-Earth object, m
r_{fi}	=	distance from spacecraft to the sun, km
S_{flux}	=	solar flux at 1 AU, 1367 W/m^2
S_{sc}	=	scattering factor
T	=	temperature, K
T_n	=	thrust, N
t	=	time, s or days
t_f	=	time at which the deviation maneuver is completed, s or days
t_{MOID}	=	time at the minimum orbit interception distance point, s or days
t_{push}	=	duration of the pushing action, s
t_0	=	time at which a low-thrust deviation maneuver begins or an impulsive maneuver occurs, s or days
$\bar{V}$	=	average velocity of evaporated particles, m/s
V_{rot}	=	rotational velocity of the asteroid equatorial surface, m/s
v	=	orbital velocity, km/s
v_{debris}	=	velocity of the debris from the nuclear Interceptor, m/s
v_e	=	excess velocity of the expelled or sublimated material, m/s
YTW	=	yield-to-weight ratio of the nuclear device, kton/kg
$Z_{\max}$	=	maximum radiation depth, m
z	=	asteroid depth, m
β	=	momentum enhancement factor
$\Delta\mathbf{r}$	=	vector distance at the minimum orbit interception distance point, km

Received 22 January 2008; revision received 24 July 2008; accepted for publication 15 August 2008.

*Ph.D. Candidate, Department of Aerospace Engineering, James Watt (South) Building; psanchez@eng.gla.ac.uk.

†Ph.D. Candidate, Department of Aerospace Engineering, James Watt (South) Building; ccolombo@eng.gla.ac.uk.

‡Senior Lecturer, Department of Aerospace Engineering, James Watt (South) Building; mvasile@eng.gla.ac.uk. Senior Member AIAA.

§Senior Lecturer, Department of Aerospace Engineering, James Watt (South) Building; gradice@eng.gla.ac.uk. Member AIAA.

$\Delta\mathbf{v}_{S/C}$ = relative velocity of the spacecraft with respect to the asteroid, m/s or km/s
$\Delta t_{shooting}$ = time available to shoot the dug material, s
$\delta\mathbf{r}$ = deviation vector in the Hill coordinate frame, km
$\delta\mathbf{v}$ = impulsive change of velocity vector, m/s or km/s
δv = scalar increment of velocity, m/s or km/s
ε = elevation angle, deg
ε_{bb} = blackbody emissivity
η = spacecraft-centered nadir angle, deg
η_{eff} = efficiency of the mirror assembly
θ = true anomaly of an orbit, deg
θ^* = argument of latitude of an orbit, deg
κ = thermal conductivity, W/m/K
λ = asteroid central angle, deg
μ_o = opacity of a material to a certain radiation, m^2/kg
ν = angle between the orbital velocity and the axis of the ecliptic inertial reference frame, deg
ξ = specific thrust, N/W
ρ_a = mean density of the asteroid, kg/m^3
σ = Stefan–Boltzmann constant, 5.67051×10^{-8} $W/m^2/K^4$
τ = mass-to-power ratio, kg/W
ϕ = exhaust cone half-angle, deg
Ω = argument of the ascending node of an orbit, deg
ω = argument of the perigee of an orbit, deg
ϖ = complementary latitude angle, deg

Subscripts

h = vector component normal to the orbit plane
n = vector component normal to the orbit in the orbit plane
t = vector component tangent to the orbit

I. Introduction

OVER the last few years, the possible scenario of an asteroid threatening to impact the Earth has stimulated an intense debate among the scientific community about possible deviation methods. Small celestial bodies such as near-Earth objects (NEOs) have become a common subject of study because of their importance in uncovering the mysteries of the formation, evolution, and composition of the solar system. Among all asteroids, NEOs have stepped into prominence because of two important aspects: they are among the easiest celestial bodies to reach from Earth, in some cases they can be reached with less demanding trajectories than a simple Earth–moon trajectory, and, even more meaningful, they may represent a threat to our planet.

On average, every 26–30 million years a 10-km-sized asteroid strikes the Earth, and every several hundred years there is a Tunguska-class (100 m in diameter) asteroid impact [1]. Each of these impacts permanently alters the characteristics of our planet to varying degrees. These events, and the risks they pose to our fragile ecosystem, have made the space community turn their attention to the NEO issue [2].

Evidence of this newfound interest is the prolific and successful asteroid exploration program of the last decade, with many completed missions such as Near-Earth Asteroid Rendezvous, Deep Space 1, Deep Impact, or Stardust; ongoing missions such as Rosetta, Hayabusa, and Dawn; and future missions such as Don Quijote, which will not only study the target asteroid, but will also test the capability to deflect its course with a high-velocity impact.

To predict the effects of a deflection strategy, some studies have addressed the asteroid deviation problem either with an analytical approach [3,4] or by means of a numerical procedure based on a n-body model [5]. Previous deflection formulas considered only a change in the orbital period due to an action applied along the direction of the motion of the asteroid. A more general approach was proposed by Conway [6] to determine the near-optimal direction in which the impulse should be applied to maximize the consequent deviation. A similar approach was taken by Park and Ross [7], who also took into consideration the gravitational effects of the Earth [8], obtaining a more accurate estimation of the optimal impulse.

A few authors have performed a partial comparative assessment of the numerous proposed mitigation strategies. Some of these emphasize a classification system based on NEO/spacecraft coupling [9], other systems are based on technology readiness, and a third category is based on time to impact and/or intervention of the asteroid. On the other hand, since the day the first mitigation technique [10] was proposed, many approaches have been put forward by several scientists and a comprehensive quantitative comparison is still lacking.

All of these different techniques can be grouped into several families, depending on the type of asteroid-spacecraft interaction: techniques producing an impulsive change in the linear momentum of the asteroid, such as kinetic impactors and nuclear interceptors [11–13]; techniques actively producing a controlled continuous low thrust, such as attached propulsion devices [4] (e.g., electric/chemical engines and solar sails) or gravitational tugs [14]; techniques producing a passive low thrust by an induced change of the thermo-optical properties of the asteroid surface [15], such as the enhanced Yarkovsky effect or enhanced emissivity through white paint; techniques producing a controlled thrust by the ablation of the asteroid surface [16] (e.g., through laser beams or solar collectors); or techniques producing a multi-impulsive change of the asteroid linear momentum by the ejection of surface material, such as the mass driver [17].

This paper presents a comparison of deflection methods according to a set of different criteria. A collection of NEOs differing in physical characteristics (i.e., size, mass, and spin properties) and orbital parameters was selected for this analysis. A group of different mitigation strategies taken from the preceding listed families was then applied to these asteroids and evaluated in terms of four figures of merit: achieved miss distance at the Earth, warning time, total mass into orbit, and technology readiness level (i.e., the estimated time to develop the technology required to implement a given mitigation strategy).

The first three criteria (miss distance, warning time, and mass into orbit) quantitatively express how easy it is to deflect an asteroid with a given method and whether we can implement a given deviation strategy with present launch capabilities. The warning time, in particular, in addition to giving quantitative information on the time to react (how far in advance we need to know that an impact is going to occur), gives an indication of the time available to repair a failed deflection operation.

Finally, the paper presents a multicriteria optimization that provides a preliminary and relative measure of the effectiveness of one deviation over another according to the selected criteria.

II. Deviation Formulas and Maximum Deviation Problem

Given the minimum orbit interception distance point (MOID) from the Earth for a generic near-Earth object, the objective is to maximize the MOID by applying a deviation action. The effect on the asteroid of all of the deviation strategies in this paper was modeled either as an impulsive $\Delta\mathbf{v}$ at the interception time t_0 or as a continuous acceleration over the interval t_0–t_f, where t_f is the time in which the deviation maneuver is completed. The achieved miss distance is computed by means of proximal motion equations [18] expressed as a function of the variation of the orbital elements. The variation of the orbital elements is computed with Gauss's planetary equations [19].

The deviation maneuver acts as a perturbation on the orbit of the asteroid, and the new orbit can be considered proximal to the unperturbed orbit. If θ_{MOID} is the true anomaly of the NEO at the MOID point along the unperturbed orbit and $\theta^*_{MOID} = \theta_{MOID} + \omega$ is the corresponding argument of latitude, we can write the variation of the position of the NEO, after deviation, with respect to its unperturbed position by using the proximal motion equations:

$$
\begin{aligned}
\delta s_r &\approx \frac{r}{a}\delta a + \frac{ae\sin\theta_{\mathrm{MOID}}}{\eta}\delta M - a\cos\theta_{\mathrm{MOID}}\delta e \\
\delta s_\theta &\approx \frac{r}{\eta^3}(1+e\cos\theta_{\mathrm{MOID}})^2\delta M + r\delta\omega \\
&\quad + \frac{r\sin\theta_{\mathrm{MOID}}}{\eta^2}(2+e\cos\theta_{\mathrm{MOID}})\delta e + r\cos i\delta\Omega \\
\delta s_h &\approx r(\sin\theta^*_{\mathrm{MOID}}\delta i - \cos\theta^*_{\mathrm{MOID}}\sin i\delta\Omega)
\end{aligned}
\tag{1}
$$

where δs_r, δs_θ, and δs_h are the displacements in the radial, transversal, and perpendicular-to-the-orbit-plane directions, respectively, so that $\delta\mathbf{r} = [\,\delta s_r \quad \delta s_\theta \quad \delta s_h\,]^T$ and $\eta = \sqrt{1-e^2}$.

In the case of an impulsive action on the asteroid, the variation of the orbital parameters a, e, i, Ω, and ω between the unperturbed and the proximal orbit are computed through Gauss's planetary equations written for an instantaneous change in the NEO velocity vector $\delta\mathbf{v} = [\,\delta v_t \quad \delta v_n \quad \delta v_h\,]^T$, where the components of this vector are expressed in the tangential, normal, and perpendicular-to-the-orbit-plane directions at $\theta = \theta_0$,

$$
\begin{gathered}
\delta a = \frac{2a^2 v}{\mu}\delta v_t \qquad \delta e = \frac{1}{v}\left[2(e+\cos\theta_0)\delta v_t - \frac{r}{a}\sin\theta_0\delta v_n\right] \\
\delta i = \frac{r\cos\theta^*_0}{h}\delta v_h \qquad \delta\Omega = \frac{r\sin\theta^*_0}{h\sin i}\delta v_h \\
\delta\omega = \frac{1}{ev}\left[2\sin\theta_0\delta v_t + \left(2e + \frac{r}{a}\cos\theta_0\right)\delta v_n\right] - \frac{r\sin\theta^*_0\cos i}{h\sin i}\delta v_h
\end{gathered}
\tag{2}
$$

and with the total variation in the mean anomaly:

$$
\begin{aligned}
\delta M &= -\frac{b}{eav}\left[2\left(1+\frac{e^2 r}{p}\right)\sin\theta_0\delta v_t + \frac{r}{a}\cos\theta_0\delta v_n\right] \\
&\quad + \delta n(t_{\mathrm{MOID}} - t_0)
\end{aligned}
\tag{3}
$$

Equation (3) takes into account the instantaneous change of the orbit geometry at time t_0 and the change in the mean anomaly at the time of the MOID due to a change in the semimajor axis, given by $\delta n(t_{\mathrm{MOID}} - t_0)$, where t_{MOID} is the time at the MOID point along the orbit of the NEO and

$$
\delta n = \sqrt{\frac{\mu}{a^3}} - \sqrt{\frac{\mu}{(a+\delta a)^3}}
$$

When a continuous deviation action is selected instead, the total variation of the orbital parameters is computed by numerically integrating Gauss's variational equations over the interval t_0–t_f, applying the acceleration produced by the deviation strategy. In this case, the variation of the mean anomaly is computed in a similar fashion to Eq. (3):

$$
\delta M = (n_f - n)t_{\mathrm{MOID}} + nt_0 - n_f t_f + \Delta M \tag{4}
$$

where n is the nominal angular velocity, n_f is the mean motion at time t_f, and ΔM is calculated through the numerical integration of Gauss's equations.

III. Asteroid Deflection Strategies

In this paper, we analyze and compare six deflection strategies: solar collector, nuclear interceptor, kinetic impactor, low-thrust propulsion, mass driver, and gravity tug. To study the effectiveness of each deviation strategy, a set of mathematical models was developed to compute the variation of the linear momentum of a NEO, due to each one of the deviating actions. The deviating action produced by kinetic impactor and nuclear interceptors was modeled as an impulsive variation of the NEO's velocity, and the deviating actions provided by low-thrust propulsion, gravity tug, and solar collector were modeled as a continuous variation of the asteroid linear momentum. The effect of mass drivers was instead modeled as a sequence of impulses and thus as a discrete variation of the linear momentum of the asteroid.

It is assumed that the direction of the deviating impulse for kinetic impactors and nuclear interceptors depends only on the transfer trajectory from the Earth to the asteroid and is aligned with the relative velocity vector between the spacecraft and the asteroid at the end of the transfer. For all of the other strategies, the direction of the deviating action is instead independent of the transfer, and thus we chose the closest direction to the theoretical optimal direction [20].

The remainder of this section contains a description of the mathematical models for the six aforementioned deviation methods. Some of the models are taken from the existing literature and adapted to the present analysis and others represent a new development with respect to what is already in the literature.

A. Nuclear Interceptor

Nuclear devices are able to carry the highest energy density among all of the deviation methods currently available. Not surprisingly, the first deviation strategy ever proposed [10] already suggested the use of nuclear bombs to change the collision course of an asteroid. On the other hand, it is worthwhile to remark that this technology could represent a significant risk. As pointed out by Sagan in [21], all mitigation technologies can be a double-edged sword if misused, but for obvious reasons, delivering nuclear warheads in space could represent a higher menace than other deflection methods. This fearsome risk, intrinsic to this technology, would most probably raise political and security issues, which would certainly make the development of deflection strategies based in nuclear weapons more than a technological problem. However, the work described here has not considered those additional issues.

The model used in this study is based on a standoff configuration over a spherical asteroid. This type of configuration requires detonating the nuclear charge at distance H from the asteroid surface (Fig. 1). The method is less sensitive to possible uncertainties in the asteroid composition and surface morphology [22], unlike other nuclear-based configurations, such as buried and surface explosions. The energy released during a nuclear explosion is carried mainly by x-rays, neutrons, gamma radiation, and debris, and its distribution depends mostly on the type of nuclear reaction.

Table 1 shows the distribution of energy used in this work, which is taken from Hammerling and Remo [22] and is based on the information by Glasstone [23]. As can be read in the table, an important part of the total energy is carried, in the form of kinetic energy, by the debris resulting from the explosion. Although its momentum coupling, or efficiency in producing linear momentum change, is much smaller than that of the radioactive processes (as will be seen later), its effect cannot be neglected. In the following, a model for the computation of the change in the velocity of the asteroid due to debris and radiation is presented.

1. Debris

After the detonation of the nuclear device, part of the debris from the spacecraft structure and components will impact the surface of the asteroid. Assuming that the explosion produces a spherical shock wave and the debris is homogeneously distributed on the surface of

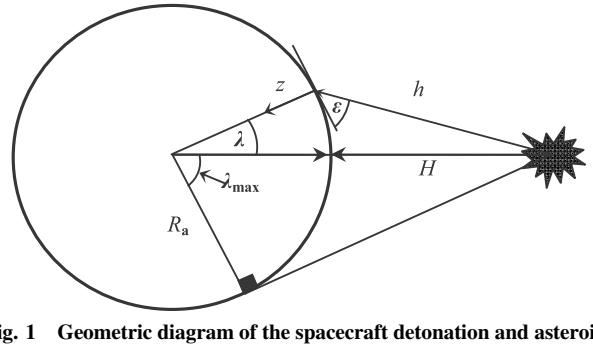

Fig. 1 Geometric diagram of the spacecraft detonation and asteroid.

Table 1 Energy distribution

Source	X-ray	Neutrons	Gamma rays	Debris	Others
Fission	70%	1%	2%	20%	7%
Fusion	55%	20%	1%	20%	4%

this shock wave, the total amount of debris impacting the asteroid m_{debris} is given by the dry mass of the spacecraft m_d multiplied by the ratio S between the total area of the shock wave and the portion of it that intersects the asteroid:

$$m_{\text{debris}} = Sm_d \tag{5}$$

where S is defined as

$$S = \frac{1}{2} - \frac{\sqrt{H}}{2}\frac{\sqrt{H+2R_a}}{R_a+H} \tag{6}$$

Here and in the following, the dry mass m_d is the mass of the spacecraft without the propellant to perform the transfer from the Earth to the asteroid. The impacting velocity of the debris v_{debris} is then given by

$$v_{\text{debris}} = \sqrt{\frac{2f_{\text{debris}}E_t}{m_d}} \tag{7}$$

where E_t is the total yield release by the nuclear interceptor, and f_{debris} is the fraction of delivered energy in kinetic form (see Table 1). The final increment in the asteroid velocity δv_{debris} is calculated by using the conservation of linear momentum:

$$\delta v_{\text{debris}} \approx \beta S_{\text{sc}}\frac{m_{\text{debris}}v_{\text{debris}}}{M_a} \tag{8}$$

where S_{sc} is a scattering factor, β is the momentum enhancement factor [11], and M_a is the mass of the asteroid.

2. Radiations

Following the Beer–Lambert law of absorption, the radiant energy absorbed per unit area by a layer of material of thickness $\mathrm{d}z$ and mass per unit area $\mathrm{d}m_A = \rho_a\,\mathrm{d}z$ is

$$\mathrm{d}E_A = -\mu_0 E_A\,\mathrm{d}m_A \tag{9}$$

where μ_o is the opacity of the material; E_A is the received energy per unit area; ρ_a is the mean density of the asteroid; and opacity μ_0, or linear mass-absorption coefficient, describes how the energy is absorbed as it passes through the asteroid, and its value depends on the radiation type, the associated energy, and the material considered. In this study, we assumed that the asteroid's surface was mainly made of forsterite and that the energy of the impacting radiation was in the range of 10 keV for x-ray, 2 MeV for gamma ray, and 14 MeV for neutron radiation [22]; with these hypotheses, the opacity for different radiations has the values in Table 2.

Thus the energy per unit area varies with the depth z is

$$\frac{\mathrm{d}E_A}{\mathrm{d}z} = -\mu_o\rho_a E_A \tag{10}$$

which, when integrated over z, gives the amount of energy per unit area remaining at a given depth:

Table 2 Opacity μ_0, or linear mass-absorption coefficient, for an asteroid made of forsterite

Radiation type	Values
X-ray	1.5 m^2/kg
Neutron	0.0044 m^2/kg
Gamma ray	0.005 m^2/kg

$$E_A(z) = E_A(0)e^{-\rho_a\mu_o z} \tag{11}$$

where $E_A(0)$ is the energy on the external surface, which depends on the distance from the explosion. The absorbed energy at a specific depth z per unit area and unit mass, $\mu_o E_A(z)$, induces the sublimation of material. A portion E_v of the energy goes into the sublimation process (sublimation enthalpy), and the remaining energy is converted into kinetic energy and accelerates the sublimated material up to a velocity v_e, given by

$$v_e = \sqrt{2(\mu_o E_A(z) - E_v)} \tag{12}$$

If we consider forsterite (i.e., Mg_2SiO_4) as the main component of the asteroids, then the sublimation enthalpy is $E_v = 5.03$ kJ/g (Wang et al. [24]). This assumption is likely to represent a worst-case scenario, because the surface of the asteroid might have more volatile materials, and the regolith may even help to increase the thrust/energy efficiency. The variation of the linear momentum per unit area $\mathrm{d}p_A$ gained by the asteroid due to the evaporated mass is

$$\mathrm{d}\,p_A = \rho_a v_e\,\mathrm{d}z \tag{13}$$

which, when integrated from the surface of the asteroid to the maximum depth at which the evaporation takes place, $Z_{\max}$, gives the total linear momentum per unit area:

$$P_A = \int_0^{Z_{\max}} dp_A\mathrm{d}z \tag{14}$$

The maximum depth $Z_{\max}$ can be computed as follows:

$$Z_{\max} = \frac{1}{\rho_a\mu_o}\ln\left(\frac{\mu_o E_A(0)}{E_v}\right) \tag{15}$$

Taking into account the elevation angle ε of the incoming radiation (see Fig. 1), the linear momentum per unit area p_A becomes

$$P_A = \int_0^{Z_{\max}\cdot\sin\varepsilon} \rho_a\sqrt{2(\mu_o E_A(0)e^{-\rho_a\mu_0\frac{z}{\sin\varepsilon}} - E_v)}\,\mathrm{d}z \tag{16}$$

The integration of Eq. (13), but without the velocity v_e, gives the mass ablated from the asteroid surface:

$$m_{\text{ablated}} = \int_0^{Z_{\max}\cdot\sin\varepsilon} \rho_a\,\mathrm{d}z \tag{17}$$

Equation (16) can now be integrated over the entire radiated surface. Using the equation of the surface of a spherical cap (see Fig. 2),

$$S_{\text{cap}} = 2\pi R_a^2(1-\cos\lambda) \tag{18}$$

we obtain an integration only dependant on the asteroid central angle λ, which leads to the following double integration:

$$P = \sqrt{8}\pi R_a^2\rho_a\int_0^{\lambda_{\max}}\left(\int_0^{Z_{\max}\cdot\sin\varepsilon(\lambda)} \times\left(\mu_o\frac{f_{\text{radiation}}E_t}{4\pi[h(\lambda)]^2}e^{-\frac{\rho_a\mu_o z}{\sin\varepsilon(\lambda)}} - E_v\right)^{1/2}\mathrm{d}z\right)\sin\lambda\,\mathrm{d}\lambda \tag{19}$$

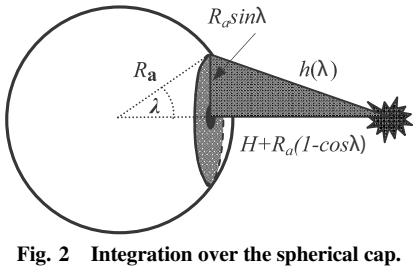

Fig. 2 Integration over the spherical cap.

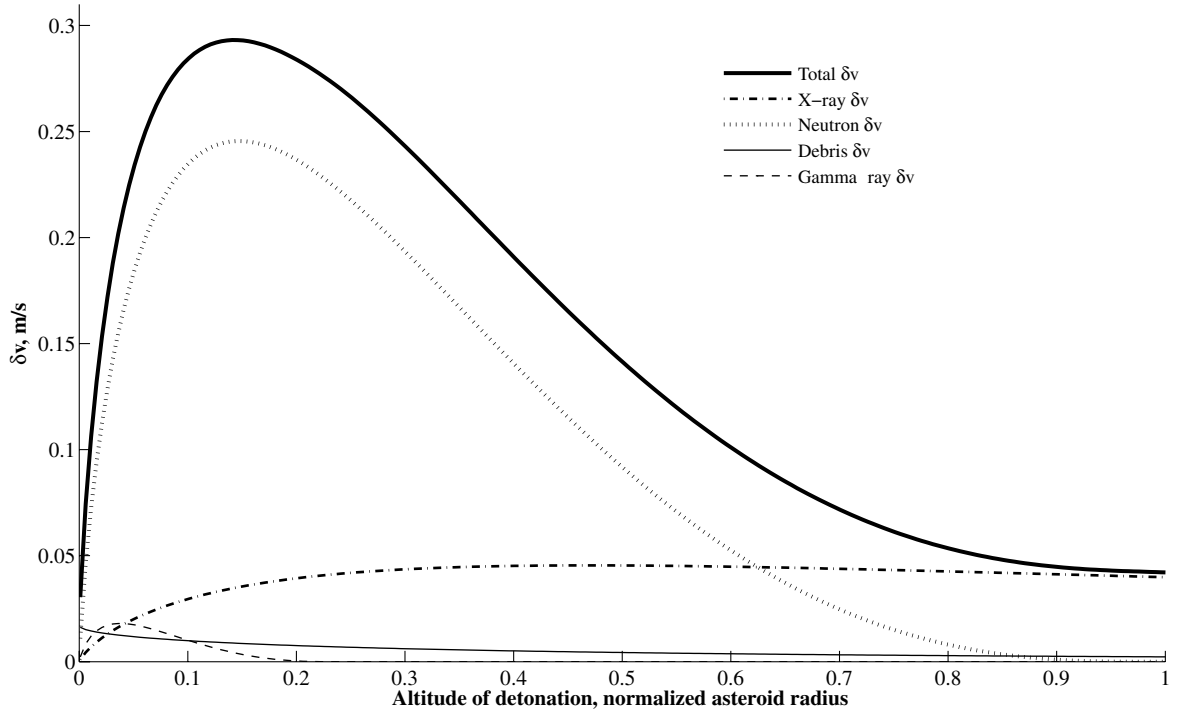

Fig. 3 Change in velocity of asteroid Apophis achieved with a nuclear interceptor carrying a fusion device of 600 kg, as a function of altitude of detonation H. The distance is normalized using the asteroid average radius.

where E_t is the total energy released by the explosion, $f_{\text{radiation}}$ is the fraction of energy corresponding to each one of the three radiations in Table 1, and h is the distance from the explosion to the surface of the asteroid. The distance h is expressed as a function of the central angle $\lambda \in [0 \quad \lambda_{\max}]$ (see Fig. 1), in which $\lambda_{\max}$ corresponds to the distance to the horizon of the asteroid as seen from the spacecraft. Finally, the $\delta v_{\text{radiation}}$ experienced by the asteroid is calculated by integrating Eq. (19) and dividing it by the total mass of the asteroid.

Figure 3 shows the total δv given by the combination of all four components (i.e., x-ray, neutron radiation, gamma radiation, and debris), as well as the individual contribution of each as a function of H. In this example, the spacecraft was carrying a nuclear fusion device with a mass of 600 kg in the proximity of the asteroid Apophis. Figure 3 shows that the neutron radiation gives the highest contribution to the total δv; note that the same conclusion is valid even for a nuclear fission device. The optimal standoff distance is $H = 0.15R_a$, where the maximum total increment of velocity occurs.

The ablated mass m_{ablated} and the average velocity of the sublimated material coming from each one of the types of radiation are plotted in Fig. 4. It can be observed that x-rays produce very high

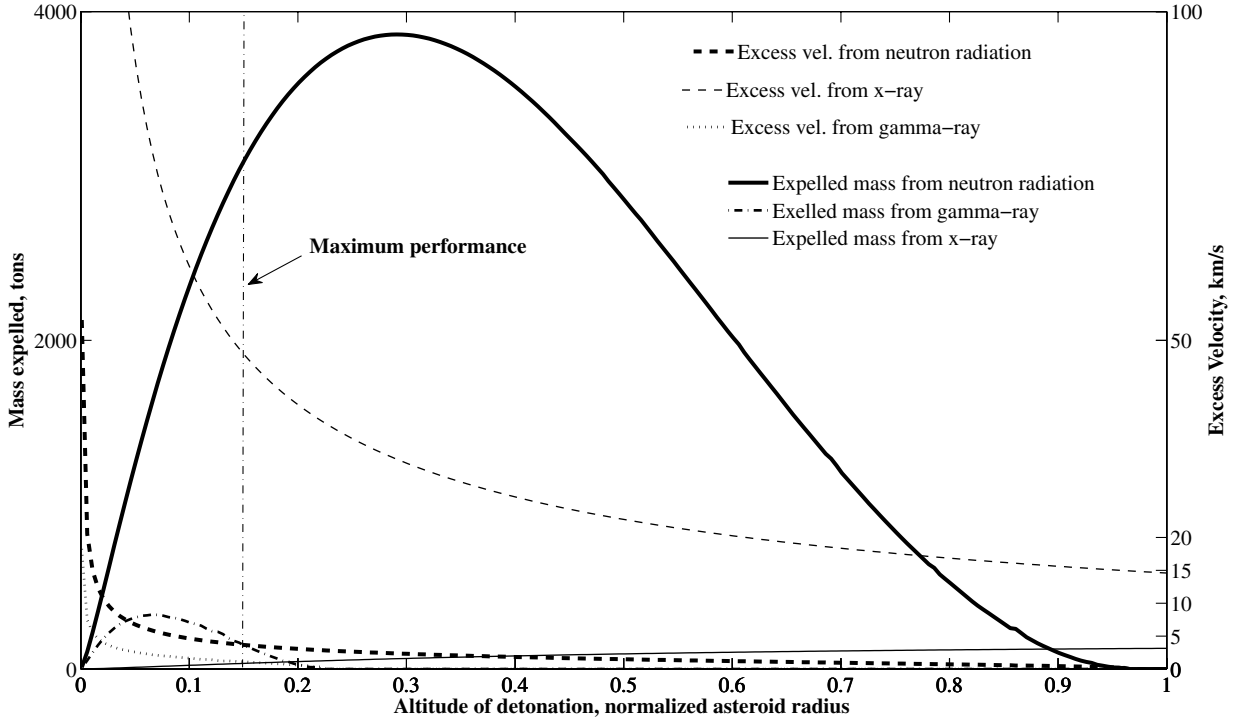

Fig. 4 Radiation analysis: Y axis on the left shows the mass evaporated by the three main radiation components of the nuclear explosion, Y axis on the right shows the excess velocity of the material that have been evaporated, and X axis is the asteroid-radius-normalized altitude of detonation.

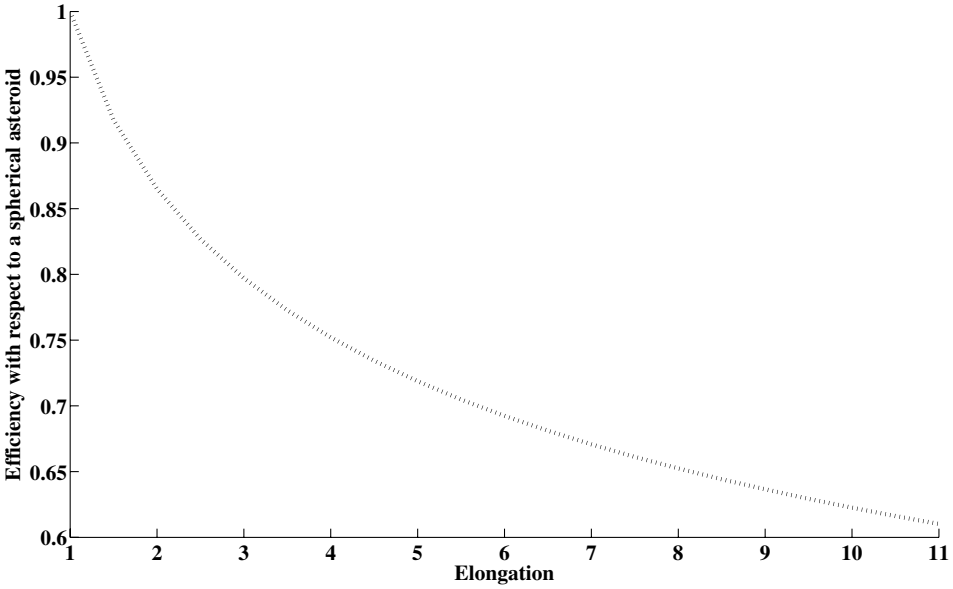

Fig. 5 Efficiency of the nuclear deflection for an elongated body. Nuclear detonation occurs over the side with the minimum cross-sectional area.

excess velocities but ablate a very thin layer of material from the surface of the asteroid. On the other hand, neutron radiation produces more evaporation, because this radiation penetrates deeper into the asteroid, and this is a more efficient way of providing impulse to the asteroid. The total impulsive action is therefore the sum of all of the individual contributions:

$$\delta v = \delta v_{\text{gamma}} + \delta v_{\text{x-rays}} + \delta v_{\text{debris}} + \delta v_{\text{neutrons}} \tag{20}$$

Note that although the core of the model developed here is based on the radiation coupling model found in the work of Hammerling and Remo [22], the numerical integration of Eq. (19) allowed us to perform a more general analysis of the nuclear option. For example, the optimal standoff distance found by Harmmerling and Remo is $H = (\sqrt{2} - 1)R_a$, which is worked out by maximizing the sum of two fractions: the energy disposed over the asteroid against the total energy and the radiated surface against the total asteroid surface, whereas the optimal detonation distance in our model is much smaller ($H = 0.15R_a$), which is driven by an optimal combination of excess velocity and mass expelled due to the nuclear radiation.

As a final consideration on the model developed in this section, we see from Eqs. (18) and (19) that the total momentum change is dependent on the area radiated by the nuclear device and on the elevation angle. The radiated area and the elevation angles depend on the shape of the asteroid. If the asteroid is not spherical but is an elongated body with the same mass, the worst-case scenario is when the explosion occurs over the side of the asteroid with the smallest cross-sectional area. To evaluate the loss of efficiency in the worst-case scenario, we computed the ratio between the total Δv for an elongated asteroid and the momentum change for a spherical asteroid with equal mass. Figure 5 shows the Δv ratio as a function of the elongation. Considering the typical measured elongation of known asteroids, the maximum expected value is 2.5 for asteroid Geographos,[¶] which corresponds to an 18% reduction in the performance of the nuclear interceptor.

3. *Spacecraft System Definition*

Finally, it is assumed that a spacecraft is carrying a nuclear device with a mass $m_{\text{wh}} = 0.3m_d$. Figure 3 shows the importance of maximizing the neutron radiation; therefore, a fusion device is chosen as the primary payload, because its fraction of nuclear radiation is considerably higher (see Table 1). The energy delivered by the explosion E_t can be computed as

$$E_t = \text{YTW}m_{\text{wh}} \tag{21}$$

where YTW is the yield-to-weight ratio of a thermonuclear device. This parameter strongly depends on the mass of the nuclear device: the larger the mass, the higher the YTW ratio. We chose a ratio of 0.75 kton/kg as a conservative option, although it ranges from 0.6 kton/kg for a warhead of 165 kg to 2.25 kton/kg for a warhead of 4000 kg.[**]

B. Kinetic Impactor

The kinetic impactor is the simplest concept for asteroid hazard mitigation: the asteroid linear momentum is modified by ramming a mass into it. The impact is modeled as a simple inelastic collision, resulting in a change in the velocity of the asteroid multiplied by a momentum enhancement factor [11]. The enhancement is due to the blast of material expelled during the impact.

The value of the enhancement factor is extrapolated from cratering analysis, such as that performed by Holsapple [25], and hypervelocity experiments. Both studies are Earth-based experiments on a small scale and extrapolation to the asteroid size and conditions is difficult to quantify. A conservative value of 2 was chosen for all of the analysis in this paper; however, for some asteroids with particular compositions and structures, the enhancement factor could be much larger [11]. The variation of the velocity of the asteroid due to the impact is given by

$$\delta \mathbf{v} = \beta \frac{m_i}{(M_a + m_i)} \Delta \mathbf{v}_{\text{S/C}} \tag{22}$$

where β is the momentum enhancement factor, and $\Delta \mathbf{v}_{\text{S/C}}$ is the relative velocity of the spacecraft with respect to the asteroid at the deviation point.

C. Spacecraft Propulsion

A straightforward mitigation strategy could consist of a spacecraft landing on the asteroid and using its propulsion system to push the asteroid out of the impact trajectory. Either traditional chemical propulsion or low-thrust propulsion systems could be used. Chemical propulsion provides very high thrust, but the excess velocity of the exhaust gases is about 10 times lower than that of the ionized plasma of low-thrust propulsion systems; thus, it requires much more propellant to achieve the same change in the linear momentum of the asteroid. For this reason, a strategy based on a

[¶]Data available online at http://echo.jpl.nasa.gov/~lance/nea_elongations.html [retrieved 16 October 2008].

[**]Data available online at http://nuclearweaponarchive.org/ [retrieved 16 October 2008].

high-thrust chemical engine was considered to be less efficient than a strategy with a low-thrust engine.

On the other hand, for electric propulsion (or low-thrust approaches in general), the rotation of the asteroid becomes an issue. On a rotating asteroid the low-thrust system will not keep a constant pointing. The propulsion system will have to be switched on and off when the correct pointing occurs or the asteroid rotation will have to be modified so that the propulsion system can be continuously active [4]. Another issue for such a mitigation approach is the definition of an appropriate attachment system between the propelling spacecraft and the asteroid. Finally, a problem pointed out by Scheeres [26] is the formation of a transient atmosphere due to the surface operations; the combination of loose regolith and low gravity could result in a transient atmosphere of dust that could potentially affect the spacecraft mechanics and operations, leading to contingencies.

Depending on how the thrust is applied and controlled, we can subdivide the class of propulsion-based deflection methods into three subclasses: scheduled low-thrust, despin and push, and precession and push.

In the following sections, the scheduled low-thrust model will be described in detail. The other possible low-thrust techniques will be briefly outlined and then compared with the scheduled thrust option. For a detailed discussion of these alternative techniques, the interested reader can refer to the work of Scheeres and Schweickart [4].

1. *Scheduled Low-Thrust Model*

The scheduled thrust model assumes a mission in which two spacecraft land on opposite sides along the equator and thrust through the center of mass of the asteroid. By properly scheduling the periods when the engines are switched on and off, we can obtain a quasi-constant thrust and a limited scattering factor. The scattering factor takes into account the misalignment from the optimal thrusting direction.

The total thrust of the system (i.e., the thrust of both engines together) is calculated using the following linear relationship:

$$T_n = m_{\text{power}} \frac{\xi}{\tau} \tag{23}$$

where m_{power} is the mass of the power subsystem, τ is the mass-to-power ratio, and ξ is the specific thrust. The specific thrust ξ is set equal to 34 mN/kW, which represents an average value for the most common ion thrusters [27]. It is also assumed that the available power is generated by a subsystem with a mass that is 50% of the dry mass of the spacecraft, $m_{\text{power}} = m_d/2$, and is capable of delivering 40 W/kg ($\tau = 25$ kg/kW [27]).

The mass of the system at the asteroid m_i includes the propellant mass for the maneuver and the dry mass m_d of the spacecraft. Because the thrust of the propulsion system is fixed by the dry mass m_d and it will remain constant for the whole mission, the total impulse produced by the propulsion system on the asteroid can be computed as follows:

$$I_t = \int_{t_0}^{t_f} F \, \mathrm{d}t = T_n \left(\frac{t_f - t_0}{2} \right) \tag{24}$$

where $F = T_n/2$ is the net force applied to the asteroid. Now the total impulse can be computed using the variation in linear momentum produced by the ionized gas expelled from the propulsion system:

$$I_t = \int_{t_0}^{t_f} \frac{\mathrm{d}m}{\mathrm{d}t} v_e \, \mathrm{d}t = (m_d - m_i) v_e \tag{25}$$

By combining Eqs. (23–25), we can obtain the dry mass m_d as a function of the initial mass m_i and of the duration of the pushing action $t_{\text{push}} = t_f - t_0$:

$$m_d = m_i \Big/ \left[1 + \frac{\xi}{2\tau I_{\text{sp}} g_0} \frac{t_f - t_0}{2} \right] \tag{26}$$

The maneuver could be as long as the time left before the asteroid impacts the Earth, although pushing for so long is not necessarily the best strategy. Because the dry mass depends not only on the initial mass, but on the duration of the deviation maneuver as well [see Eq. (26)], it may be a better option to reduce the duration of the pushing maneuver to achieve a higher dry mass for a fixed initial mass, which translates into a better level of thrust.

An analysis of the achievable deviation as a function of the maneuver duration was carried out for six different asteroids from three different groups of NEOs: Apollo, Aten, and Amor. Assuming a constant initial mass m_i for all of the asteroids and a potential collision with the Earth in a range of 12 years, the achieved deviation was computed by numerically integrating Gauss's planetary equations over a variable pushing time.

As an example of the aforementioned analysis, Fig. 6 shows the total achieved deviation (right axis) and the total impulse (left axis) for a low-thrust deviation mission on asteroid Itokawa as a function of the percentage α of the total time available for applying the deviating action. The mass of the spacecraft at the beginning of the pushing action was assumed to be $m_i = 10,000$ kg, and the maximum available pushing time was fixed in this case to 10 years. The result in Fig. 6 shows how the maximum deviation is not achieved when the spacecraft is pushing for the whole available time before the collision. It is instead more convenient to use a higher thrust for a shorter time.

The result in Fig. 6 suggests a pushing maneuver that stops after the last perigee passage before 45% of the time between the arrival at the asteroid t_0 and the impact date. This prediction of the length of the pushing action matches the maximum deviation of the six studied cases with less than 2% error. Given the duration of the maneuver, the mass of propellant and the thrust can be calculated with Eq. (26).

2. *Efficiency of the Scheduled Thrust*

To measure the efficiency of the scheduled thrust compared with a full continuous thrust directed along the optimal direction, we can define the scattering factor:

$$S_f = \frac{\int_0^{1_{\text{rotation}}} (\mathbf{F} \cdot \hat{v}) \, \mathrm{d}t}{\int_0^{1_{\text{rotation}}} \mathbf{F}_{\text{optim}} \, \mathrm{d}t} \tag{27}$$

where the integrations are along one complete asteroid rotation l_{rotation}, $\hat{v}$ is the unit vector along the optimal thrusting direction, $\mathbf{F}$ is the force vector delivered by the propulsion system landed on the asteroid, and $\mathbf{F}_{\text{optim}}$ is a force vector with equal modulus but always in the optimal direction $\hat{v}$.

If we assume that the asteroid is spinning much faster than it is orbiting around the sun, we can define an asteroid orbit inertial reference frame and an asteroid equatorial inertial frame, as shown in Fig. 7. In the asteroid orbit frame, the angle ν is the angle between the orbital velocity and the $\hat{x}'$ axis; this angle will perform a complete rotation at every orbit. In the asteroid equatorial frame, the angle φ is the angle between the projection of the force vector on the $\hat{x}'\hat{y}'$ plane and the $\hat{x}'$ axis. The angle φ will perform a full revolution at every rotation of the asteroid. The obliquity of the asteroid's equator ϕ is the rotation angle necessary to transform the asteroid's orbital inertial coordinates to the asteroid equatorial inertial coordinates. Equation (27) can now be rewritten as follows:

$$S_f(\nu, \phi, \varpi) = \frac{\int_{\varphi_0}^{\varphi_f} (|F| \hat{F}(\varphi, \varpi, \phi) \cdot \hat{v}(\nu)) \, \mathrm{d}\varphi}{\int_0^{2\pi} |F| \hat{v}(\nu) \, \mathrm{d}\varphi} \tag{28}$$

where the integration limits φ_0 and φ_f are chosen so that the scalar product $\hat{F} \cdot \hat{v}$ is positive to have a constant increase in the asteroid linear momentum.

Integrating Eq. (28) along a complete orbit (i.e., ν from 0 to 2π) and dividing by 2π, we obtain an average scattering factor that depends only on the obliquity of the asteroid and the complementary latitude ϖ of the landing site. Figure 8 shows the scattering factor as a function of the obliquity angle ϕ and of the complementary latitude ϖ. The figure shows that for every obliquity, it is always possible to

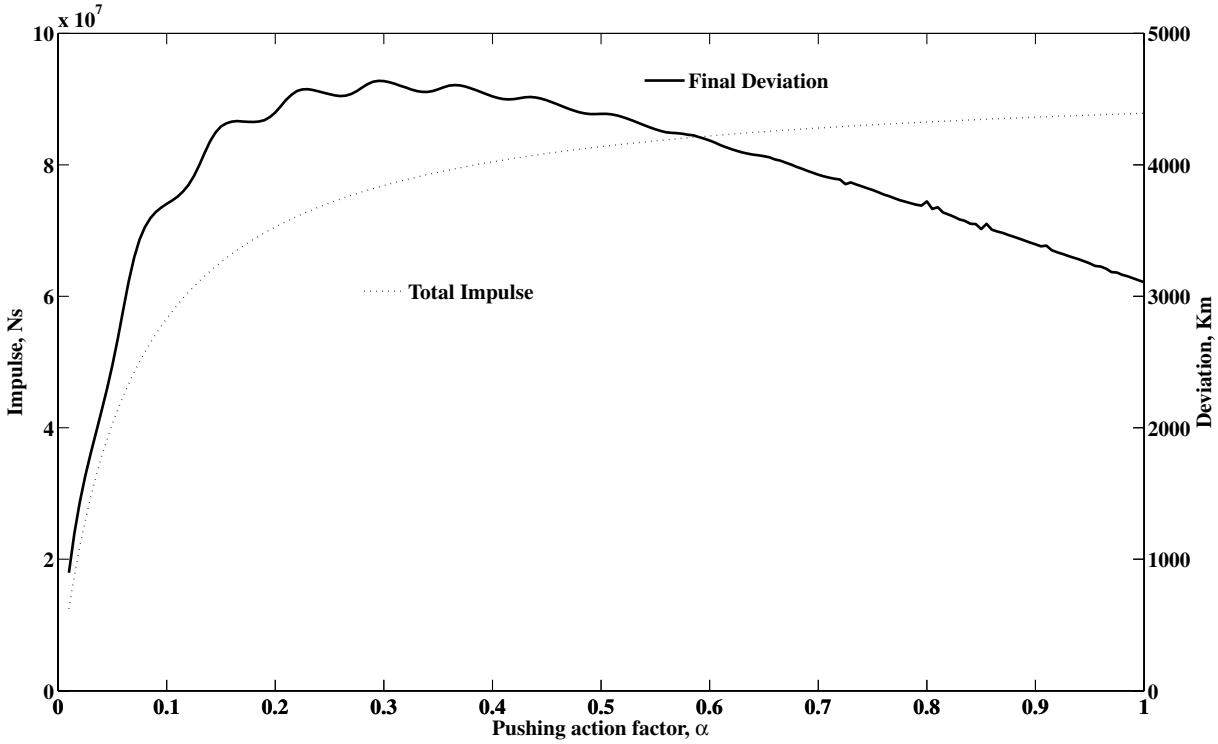

Fig. 6 Total impulse and deviation achieved for a varying α.

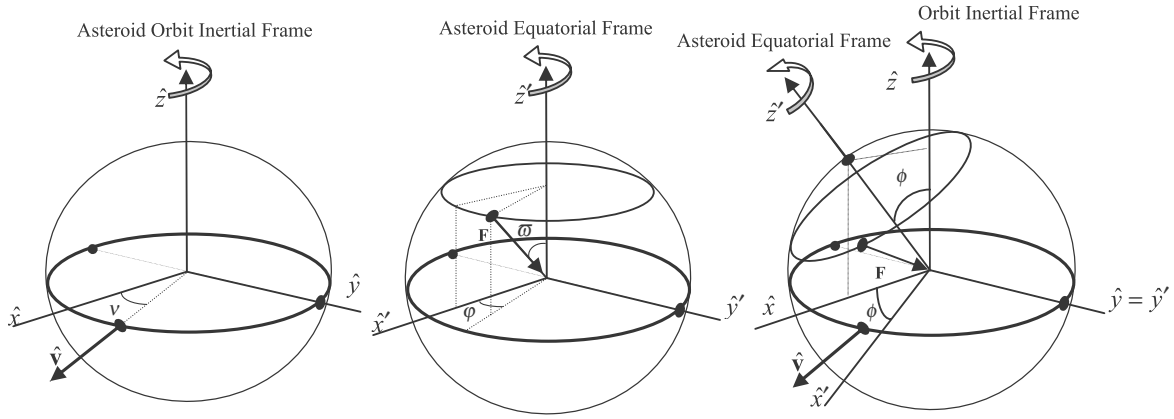

Fig. 7 Asteroid frame illustrations.

choose a landing site that guarantees a scattering factor not lower than 0.3, which means that it is always possible to have at least 30% of efficiency of thrust without changing the rotational state of the asteroid. Note that this analysis does not depend on the asteroid shape, but only on the obliquity of the asteroid's equator; thus, the efficiency of the scheduled thrust would not be affected by the asteroid shape.

3. Analysis of the Alternative Pushing Methods

Two alternatives have been suggested to solve the problem caused by the asteroid's rotation: asteroid despinning and simultaneous precession and push. Both techniques require a modification of the spinning rate of the asteroid. The despin method is a three-phase method. During the first phase, the low-thrust propulsion is used to stop the rotation of the asteroid. Next, a new rotational state is imposed to match the asteroid's orbital period. Then the propulsion system is used to push the asteroid out of the collision trajectory. The second alternative requires one to reorient the asteroid rotational pole and, as demonstrated by Scheeres and Schweickart [4], there is always an axial tilt such that it is possible to thrust continuously while maintaining a constant relative orientation between the rotational axis and the optimal thrusting direction.

Figure 9 shows the effective total impulse produced by each one of the aforementioned techniques for a wide range of thrust levels. The effective total impulse for the scheduled thrust is the product of the thrust times the scattering factor times the pushing time. The effective total impulse for the despin method instead is the thrust times the available pushing time after the despinning operations. Finally, the effective total impulse for the precession-push method is the product only of the thrust component in the direction of the asteroid velocity times the pushing time.

As it can be seen in Fig. 9, the despinning technique requires a minimum level of thrust to stop the rotation of the asteroid before the impact with the Earth. This minimum thrust level depends on the angular velocity of the asteroid's rotation and the time available for despinning and deviating the asteroid. For the analysis in Fig. 9, the maximum available time was set to 4 years for all of the low-thrust methods.

For the simultaneous precession and push, considering that the asteroid already has the proper configuration to start the deviating maneuver as soon as the spacecraft arrives, the faster the rotation, the higher the fraction of the thrust that goes into controlling the precession and hence less variation of the linear momentum for the same propellant consumption. In the remainder of this work, all

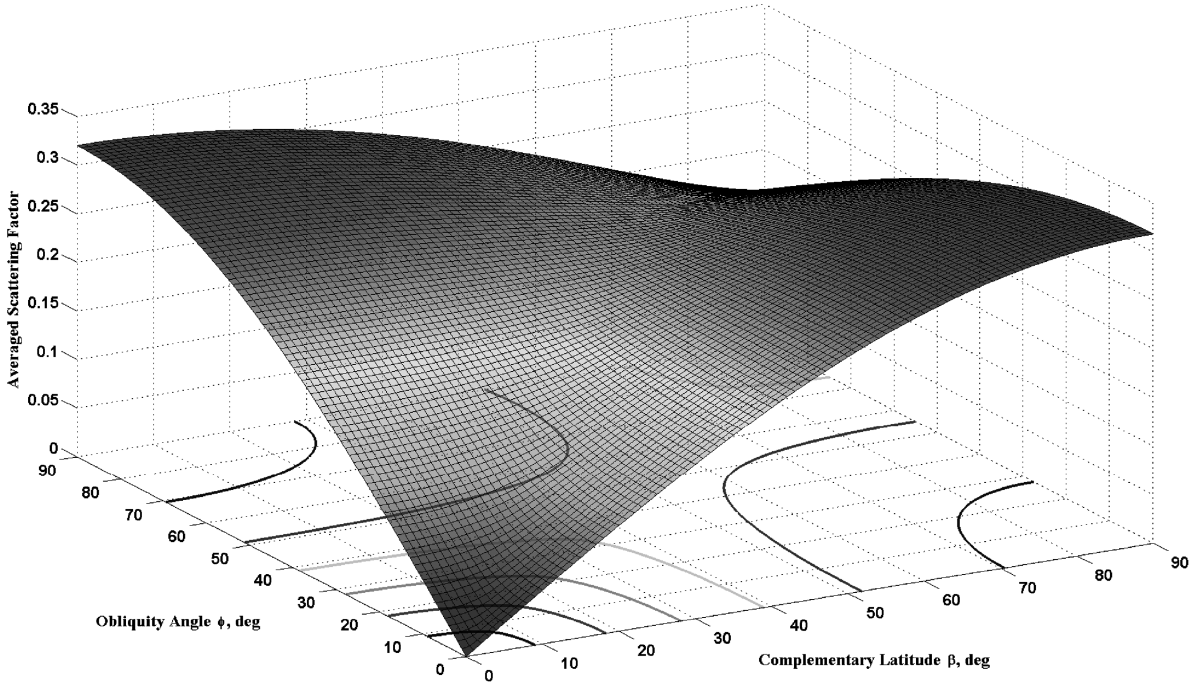

Fig. 8 Averaged scattering factor.

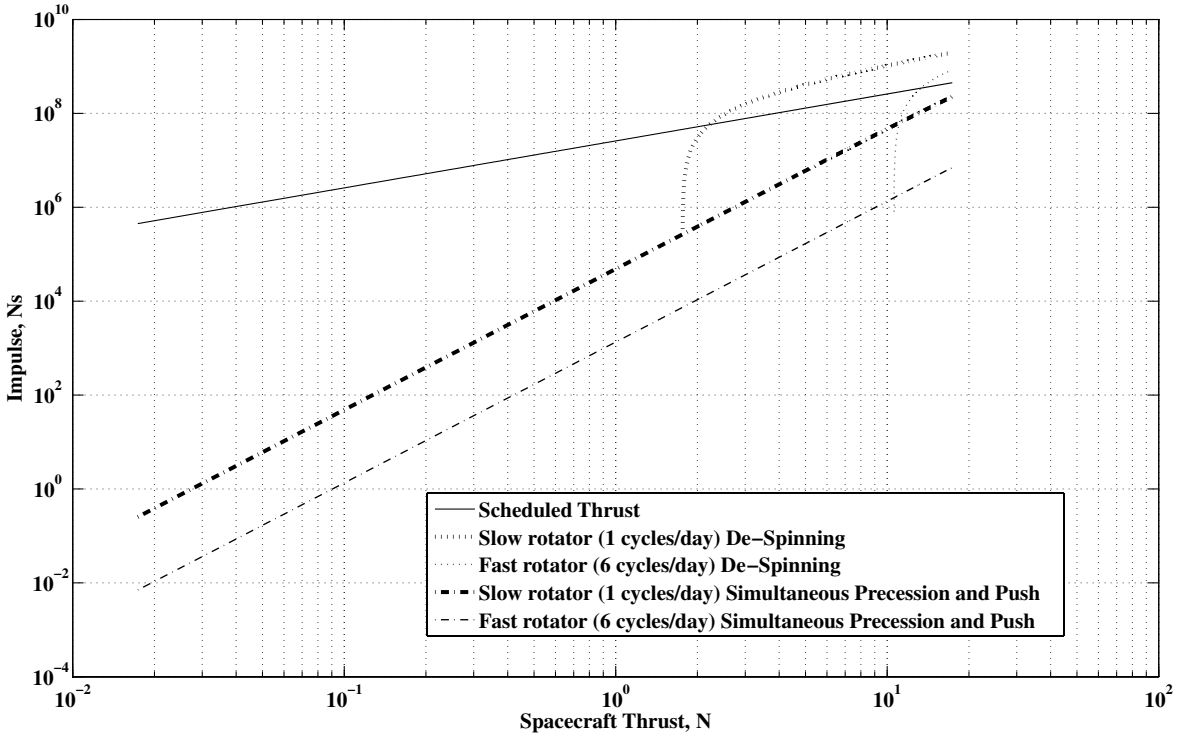

Fig. 9 Comparison among three possible low-thrust strategies for a wide range of thrust levels and 20 years of pushing time.

analyses on the low-thrust propulsion method will consider only the scheduled approach, because, as Fig. 9 shows, the scheduled thrust method performs well for all of the thrust levels, spinning rates, and available pushing time considered in this study.

D. Mass Driver

The mass driver system generates a change in the velocity vector of the asteroid by shooting pieces of the asteroid's outer crust into space. Some surface material is dug by a drilling device and accelerated into space through an electromagnetic rail gun. The advantage of this strategy is that the material used to change the linear momentum of the asteroid is obtained in situ and not carried from Earth.

The model for the mass driver was developed assuming that a spacecraft with mass m_d is landed along the equator of the asteroid and directing the rail gun along a line perpendicular to the rotation axis, which is assumed to be perpendicular to the velocity vector of the asteroid. Furthermore, it was assumed that when the rail gun is not pointing in an optimal direction, the spacecraft is collecting material. The dug material is shot once per rotation when optimal pointing conditions are met, within a given tolerance.

The mass of the power subsystem was assumed to account for 30% of the dry mass m_d, which is in agreement with the results obtained by Olds et al. [28]. The mass-to-power ratio τ was set to 25 kg/kW [27], which is an averaged value for the power sources most commonly used in space. The energy efficiency of the rail gun was set to 30% [29]; hence, approximately one-third of the electrical energy generated by the power source is transformed into kinetic energy:

$$P_K = 0.3\frac{m_{\text{power}}}{\tau} \tag{29}$$

where $m_{\text{power}} = 0.3 \cdot m_d$ is the mass of the power system, and P_K is the total power converted into kinetic energy.

In the literature, a value of 100–300 m/s is suggested as a realistic excess velocity for the expelled mass [28,30]; therefore, in this paper, an excess velocity of 200 m/s, which is within the current technological capabilities [29], was considered for all of the analysis. Given the excess velocity, the mass expelled per shot can be calculated with the following equation:

$$m_{\text{launch}} = \frac{2P_K \Delta t_{\text{shooting}}}{v_e^2} \tag{30}$$

where $\Delta t_{\text{shooting}}$ is time available to shoot the dug material into space, which was set to be equal to the time required to the pointing vector of the rail gun to span a 10 deg arc around the rotation axis of the asteroid (i.e., $\Delta t_{\text{shooting}} = 0.0278 T_{\text{rot}}$, where T_{rot} is the rotational period of the asteroid). It is assumed that power generated when the mass driver is not shooting (97% of the time) is sufficient for the mining system (e.g., a coring drill) to prepare the next projectile [31,32].

The change in the velocity of the asteroid is determined by using the conservation of linear momentum and taking into account the change in the asteroid mass consequent to every shot:

$$\delta v = \frac{m_{\text{launch}}}{M_a(t)} v_e \tag{31}$$

At each impulsive δv there is a corresponding finite variation of the orbital elements of the asteroid, and the new set of orbital parameters has to be calculated before the subsequent impulsive action.

Note that, similar to the low-thrust method, the mass driver generates a Δv only when the rail guns point in the correct direction. The performance of this method is therefore not affected by the shape of the asteroid, but by its rotational state.

E. Solar Collector

Melosh et al. [16] proposed the use of a mirror to focus the solar energy onto a small portion of the surface of the asteroid. The resulting heat sublimates the surface material, creating a jet of gas and dust that produces a continuous thrust. This thrust ultimately alters the orbit of the asteroid in a similar fashion to how a comet's orbit is altered by the expulsion of material from surface jets. A conceptually similar idea is to use a laser beam, either powered by a nuclear reactor or solar arrays, to induce the required sublimation of the surface material. In the following, a model is proposed to compute the deviating acceleration due to the flow of gases derived from the sublimation of the asteroid's surface. Although the model is applicable to both the solar collector idea and to the laser beam concept, the spacecraft model that will be employed in the following analyses assumes the use of a solar concentrator. This choice was motivated by the expected mass of the laser, together with the power unit required to operate the laser. After a first estimation, the mass of a deployable mirror proved to be smaller than the equivalent mass of the laser plus power unit. However, this does not intend to rule out the laser option; on the contrary, although a more detailed spacecraft system analysis might demonstrate that the laser option is more advantageous than the solar collector, the sublimation model presented in this section and the following analysis will maintain their validity and the resulting conclusions would be applicable to the laser case as well as to the solar case.

1. *Spacecraft Model*

It is assumed that the solar concentrator is made of a layer of reflecting material mounted on an inflatable supporting structure [33]. The inflatable structure and the deployment system, attachments, and related harnessing are assumed to account for 30% of the total dry mass of the spacecraft. From the work of Hedgepeth and Miller [34], the mass-to-area ratio of the inflatable solar concentrator is estimated to be 0.1 kg/m^2. This is a conservative estimation when compared with the size and mass of space experiments such as the Znamya and Echo balloons.

The size of the spacecraft is related to the amount of energy focused on the surface of the asteroid through the ratio between the area of the reflective surface and the area of the illuminated spot, or concentration ratio. Concentration ratios between 2000 and 3000 are possible for space solar concentrators [34]. In the following, a concentration ratio of 2500 will be used, which is equivalent to a diameter for the illuminated spot that is 50 times smaller than the diameter of the mirror.

2. *Thermal Model of an Asteroid*

If a beam of light is focused onto the surface of the asteroid, the received power density can be calculated by using

$$P_{\text{solar}} = \eta_{\text{eff}} \frac{S_{\text{flux}}}{r_{\text{fi}}^2} \frac{A_m}{A_s} (1 - \text{albedo}) \tag{32}$$

where A_m is the cross-sectional area of the reflective surface of the mirror, perpendicular to the direction of the solar radiation; A_s is the area of the illuminated surface on the asteroid; $\eta_{\text{eff}} = 90\%$ is the efficiency of the mirror assembly; $S_{\text{flux}} = 1367$ W/m^2 is the solar flux at 1 AU; r_{fi} is the distance from the spacecraft to the sun, which scales the solar flux; and the albedo was chosen as 0.2. This value approximates the albedo of an *S*-type asteroid, the surface of which is mostly composed of olivine. For the specific deviation method under investigation, an albedo of 0.2 would correspond to a worst-case scenario.

The time that a portion of the surface spends under the spot beam is a function of the angular rotation of the asteroid and of the size of the spot, which is also a function of the size of the mirror and the concentration ratio. The model assumes the system to be an infinitely long rod, with the illuminated spot on one side of it. The illuminated surface is at a temperature of 1800 K, which is the sublimation temperature of forsterites [23]. The long rod model represents a good approximation of the real system. In fact, it can be proved that the conduction loss through the perimeter of this rod is much smaller than the energy loss due to the movement of the surface (i.e., asteroid rotation with a fixed beam).

Sublimation is due to the total absorbed energy. The net absorbed energy is the total energy focused on the surface minus the radiation and conduction losses. Energy loss due to conduction can be computed by first solving the differential equation for the surface temperature T:

$$\frac{\partial^2 T}{\partial x^2} = \frac{c\rho_a}{\kappa} \frac{\partial T}{\partial t} \tag{33}$$

where c is the heat capacity (750 J/kg/K), ρ_a is the asteroid density, and κ is the thermal conductivity (2 W/m/K in this case). The thermal conductivity and heat capacity were calculated by using average values from different silicate materials on Earth, which are likely found on asteroids. Using the following initial and boundary conditions,

$$T(x,0) = T_0 = 278 \text{ K} \qquad T(0,t) = T_{\text{subl}} = 1800 \text{ K}$$

$$\lim_{x \to \infty} T(x,t) = T_0$$

and applying a Laplace transformation, the preceding differential equation can be solved to give

$$T(x,t) = T_0 + (T_{\text{subl}} - T_0) \cdot \text{erfc}\left(\frac{x}{2\sqrt{\kappa t / c\rho_a}}\right) \tag{34}$$

Finally, to calculate the conduction, the derivative of the temperature profile is calculated through a series expansion of the complementary error function $\text{erfc}(f(x))$. Therefore, with this model, the heat-flux loss by conduction Q_{cond} on the surface of the asteroid ($x = 0$) can be calculated to be

$$Q_{\text{cond}} = \frac{T_{\text{subl}} - T_0}{\sqrt{\pi t / c\kappa\rho_a}} \tag{35}$$

3. Rate of Expelled Mass

The heat generated by the sunlight will produce a flow of sublimated mass m_{exp}. Part of the energy goes into the sublimation process and part goes into the acceleration of the mass m_{exp}. The mass flow rate can be computed as

$$E_v \frac{\text{d}m_{\text{exp}}(t)}{\text{d}t} = \Delta Q = P_{\text{solar}} - Q_{\text{out}} \tag{36}$$

where E_v is the enthalpy of sublimation, $dm_{\text{exp}}(t)/dt$ is the flow of sublimated mass, and Q_{out} is the sum of the conduction heat loss Q_{cond} and the radiation heat loss Q_{rad}. The radiation heat loss Q_{rad} is defined according to the blackbody radiation formula as

$$Q_{\text{rad}} = \sigma\varepsilon_{\text{bb}} T^4 \tag{37}$$

where σ is the Stefan–Boltzmann constant, and ε_{bb} is the blackbody emissivity. Expanding the terms in Eq. (36) and solving for the mass flow gives

$$\frac{\text{d}m_{\text{exp}}}{\text{d}t} = \frac{1}{E_v}(P_{\text{in}} - Q_{\text{rad}} - Q_{\text{cond}}) \tag{38}$$

To calculate the total sublimated mass, Eq. (38) is integrated over the surface area under the illuminated spot. Note that if the mass flow rate $\text{d}m_{\text{exp}}/\text{d}t$ is negative, then there is not enough energy to sublimate the asteroid surface. Consequently, the limits of the integration have to be adjusted to avoid negative results. The horizontal surface position x and the illumination (or exposure) time can be related through the rotational velocity V_{rot}, such that $x = V_{\text{rot}} \cdot t$ and $\text{d}x = V_{\text{rot}} \cdot \text{d}t$. Therefore, the integral can be rewritten in terms of the exposure time t, where the limits of the integration t_{in} and t_{out} are the times at which the asteroid surface moves inside and outside the illuminated spot, respectively. Thus, the total mass flow is

$$(\dot{m}_{\text{exp}})_{\text{total}} = 2V_{\text{rot}} \int_0^{y_{\max}} \int_{t_{\text{in}}}^{t_{\text{out}}} \frac{1}{E_v}\left((P_{\text{in}} - Q_{\text{rad}}) - \left(\sqrt{\frac{c\kappa\rho}{\pi}}(T_{\text{subl}} - T_0)\right)\sqrt{\frac{1}{t}}\right)\text{d}t\text{d}y \tag{39}$$

4. Total Induced Acceleration

Once the flow rate of evaporated material is computed, the average velocity of the particles is determined by using the Maxwell distribution for particles of an ideal gas:

$$\bar{V} = \sqrt{\frac{8kT_{\text{subl}}}{\pi M_m}} \tag{40}$$

where M_m is the mass of a single molecule of Mg_2SiO_4 and k is the Boltzmann constant.

The acceleration achieved by the asteroid due to the sublimation a_{solar} can be calculated by dividing the thrust produced by the evaporation of the surface material and the remaining mass of the asteroid (the mass is decreasing due to the evaporation: for example, for a 100-m-diam mirror, the mass flow rate is on the order of 1 kg/s, which can have a significant effect for small asteroids), corrected with a scattering factor S_{sc}, accounting for the plume dispersion:

$$\|\mathbf{a}\| = \frac{(S_{\text{sc}} \cdot \bar{V} \cdot (\dot{m}_{\text{exp}})_{\text{total}})}{M_a(t)} \tag{41}$$

The scattering factor was computed assuming that the particles of debris and gas are accelerated uniformly over a semisphere, which corresponds to a 180 deg plume cone. By integrating the effective components of the acceleration over the semisphere, we get a value of $S_{\text{sc}} = 2/\pi$.

Figure 10 shows the effects of the radiation and conduction heat losses, as well as the thrust for a 100-m-diam mirror. In this simulation, the asteroid is assumed to have zero rotational velocity, but the exposure time varies between 0 and 30 s. As can be seen, below 10 s of exposure time, the thrust level drops significantly.

5. Influence of the Asteroid Spinning Rate

As mentioned, the exposure time (i.e., the time that the surface spends under the focused solar beam) depends strongly on the rotational speed of the asteroid. Figure 11 shows the deviation achieved with a 60 m mirror producing a deflection action on the asteroid Apophis. The deviation was computed by propagating Gauss's planetary equations for a period of two years, with the deviating action aligned with the instantaneous velocity vector of the asteroid. As can be seen in the figure, as the rotation speed increases, the achievable deflection monotonically decreases.

In light of the work of Harris [35], the most probable rotation state seems to be about 5.5 cycles/day. For this angular velocity, a mission with a 60-m-diam mirror would achieve a deviation of 14,000 km. Because the upper physical limit on the rotational speed is expected to be between 8 to 12 cycles/day [35], Fig. 11 shows that the deviation achieved with a solar collector for any possible rotational state would be at least 70% of the deviation achieved for a 5.5 cycles/day rotator. The upper limit on the rotational speed is assumed to be due to the rotational upper limit for asteroids without cohesive or tensile strength (i.e., rubble piles).

Finally, the elongation of the asteroid combined with its rotational state can affect the performance of this deflection method, because the distance of the target spot on the surface of the asteroid from the mirror can vary with time. However, we can assume that the focal point of the mirror can be adjusted to cope with this variation. Adapting the focal point is a technological problem that does not affect the model presented in this section, but is considered later in the paper when the technology readiness level is taken into account. A first analysis of the problem related to focusing and pointing the light of the sun can be found in other works by the authors [36,37]. In the same works, there is a preliminary analysis of the control of the mirror in proximity of the asteroid.

F. Gravity Tractor

The gravity tractor exploits the mutual gravitational attraction between an asteroid and a spacecraft to pull the asteroid off its collision course with the Earth. To perturb the asteroid in the desired way, the spacecraft should maintain a constant hovering position during the pulling period. This concept was proposed by Lu and Love [14] as a means to modify the orbit of an asteroid, overcoming the uncertainties inherent into the asteroid surface composition, morphology, and spinning rate.

The following hypotheses are used to develop the mathematical model of the gravity tractor:

1) The power subsystem accounts for 50% of the dry mass m_d.

2) The power subsystem is capable of delivering 40 W/kg ($\tau = 25$ kg/kW).

3) The propulsion subsystem generates $0.034N$/kW.

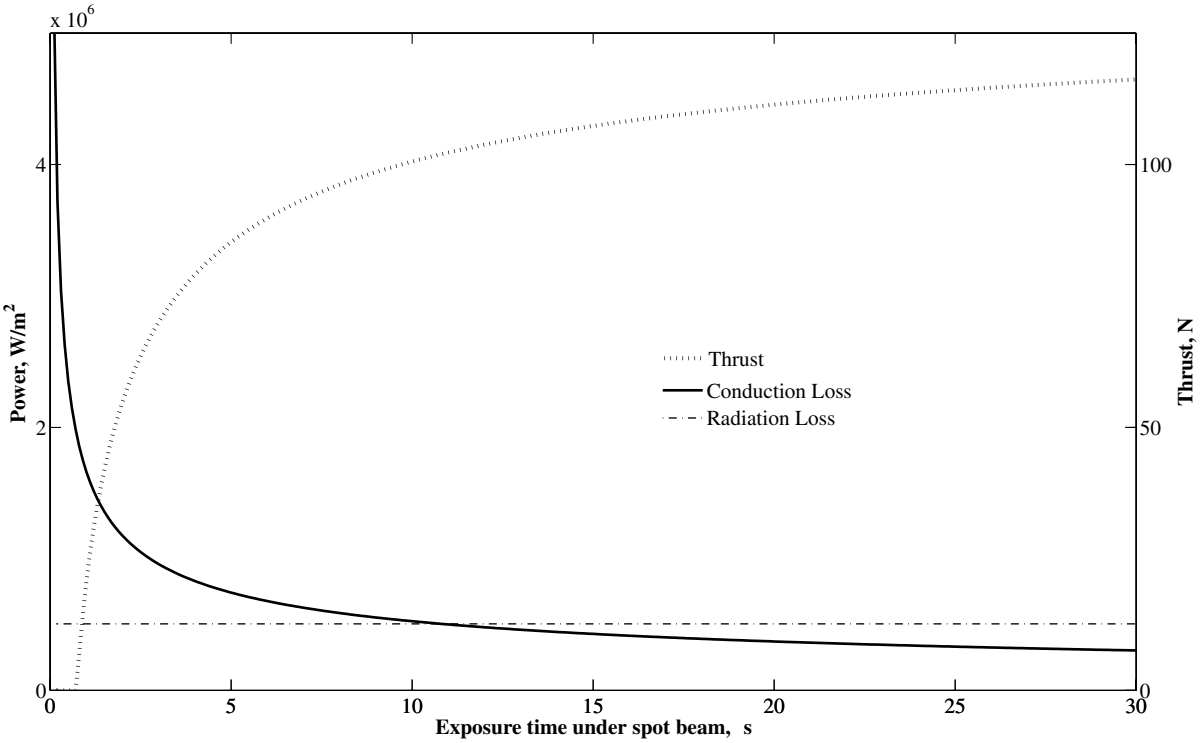

Fig. 10 Energy loss (left axis) and thrust (right axis) for a 100-m-diam mirror.

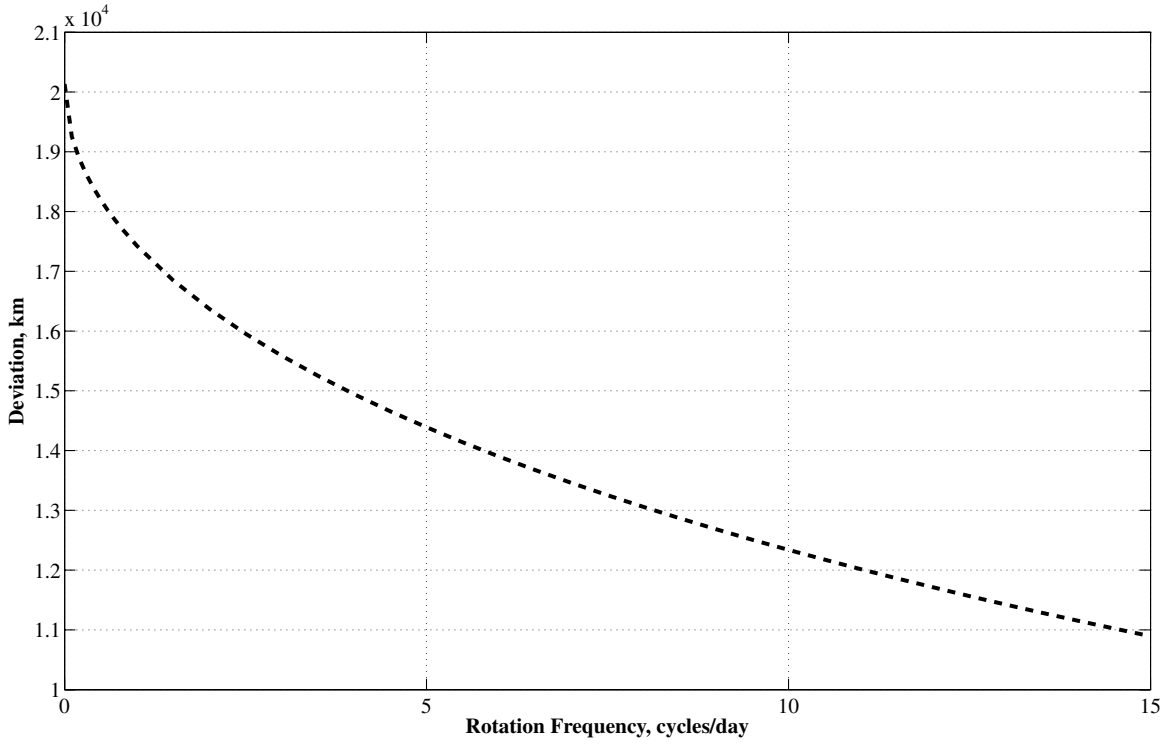

Fig. 11 Deviation as a function of the rotational speed produced by a 60-m-diam mirror acting on an Apophis-like asteroid during 2 years.

The total thrust of the spacecraft T_n is then computed by using Eq. (23). The closer the spacecraft hovers above the asteroid surface, the bigger the gravity pull. However, the exhaust gases must not impinge on the asteroid surface; otherwise, the center of mass of the NEO spacecraft system will remain unperturbed. In fact, it is the stream of mass escaping the system that generates a change in the linear momentum of the NEO [38]. Note that according to the action–reaction principle, using a specific amount of thrust to push the asteroid or using the same thrust to hover above it would lead to the same variation of the linear momentum and hence the same deviation. On the other hand, the thrusters must be properly pointed such that the cone of the exhaust gases does not intersect the asteroid surface (see Fig. 12). As a consequence, the effective vertical thrust F_{hover} is always smaller than the total thrust T_n.

As mentioned, the thrusters have to be slanted laterally by an angle ϕ equal to half the angle of the exhaust cone to avoid the impingement of the propulsion gases. With this configuration, the hovering distance can be calculated by solving the following system

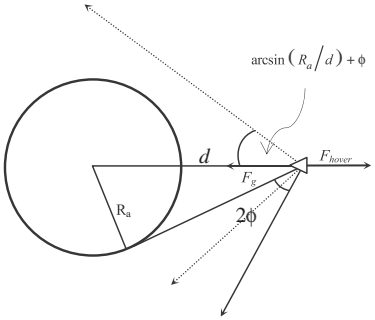

Fig. 12 Geometric diagram of the gravity tug and asteroid configuration.

of equations:

$$F_{\text{hover}} = T_n \cdot \cos\left(\arcsin\left(\frac{R_a}{d}\right) + \phi\right) \qquad F_g = \frac{GM_a m_i}{d^2} \qquad F_{\text{hover}} = F_g \tag{42}$$

where F_g is the gravity attraction between spacecraft and asteroid, F_{hover} is the thrust force in the direction of the asteroid, ϕ is 20 deg (in agreement with Lu and Love [14]), R_a is the mean radius of the asteroid, G is the universal gravity constant, M_a is mass of the asteroid, m_i is the mass of the spacecraft at the beginning of the pulling maneuver, and d is the hovering distance.

Because the spacecraft is consuming propellant to hold its hovering position, its mass will slowly decrease over time. The reduction in mass would allow the spacecraft to either hover closer to the surface or to reduce its thrust level while hovering at the same altitude. The latter option (i.e., keeping the hovering distance constant) is more advantageous because a reduction in the thrust leads to a lower propellant consumption, which in turn translates into a higher mass of the power subsystem for a fixed initial mass into space, which translates into a higher initial thrust and a lower hovering distance. By iterating this process, an optimal hovering point can be found that makes the constant-altitude option more efficient than the variable-altitude option.

If the constant-altitude option is adopted, the mass of the spacecraft at any time t during the pulling maneuver can be computed assuming a mass consumption linearly proportional to the pulling action F_{hover}:

$$m(t) = m_i e^{-\left(\frac{GM_a(t-t_0)}{d^2\cos(\arcsin(R_a/d)+\phi) I_{\text{sp}} g_0}\right)} \tag{43}$$

with the acceleration acting on the asteroid simply given by

$$a_{\text{gtug}}(t) = \frac{Gm(t)}{d^2} \tag{44}$$

Therefore, the remaining mass m_d at the end of a pulling maneuver with duration Δt_{tug} is

$$m_d = m_i e^{-\left(\frac{GM_a \Delta t_{\text{gtug}}}{d^2\cdot\cos(\arcsin(R_a/d)+\phi)\cdot I_{\text{sp}} g_0}\right)} \tag{45}$$

and by using Eq. (45) in the system of Eqs. (42), we obtain

$$\left[\left(m_i e^{-\left(\frac{GM_a \Delta t_{\text{tug}}}{d^2 I_{\text{sp}} g_0 \cos(\arcsin(R_a/d))+\phi)}\right)}\right)\Big/ 2\right]\frac{\xi}{\tau}\cos\left(\arcsin\left(\frac{R_a}{d}\right)+\phi\right) - \frac{GM_a m_i}{d^2} = 0 \tag{46}$$

which has to be solved to determine the hovering distance d.

Figure 13 shows the total impulse provided by both the low-thrust and the gravity-tug methods. Figure 13 also shows the force over the asteroid produced by these two deviation methods. For a specific low-thrust mitigation mission, the force is constant during the whole deviation maneuver; for a gravity-tug mission, the force instead decreases as a function of the mass of the spacecraft. It is interesting to note that for pulling maneuvers longer than 13 years, the force initially exerted by the gravity tug is higher than the force exerted by a low-thrust spacecraft with equal initial mass m_i. On the contrary, the total impulse is higher for the low-thrust method for deviation actions shorter than 135 years, the moment at which the total impulse

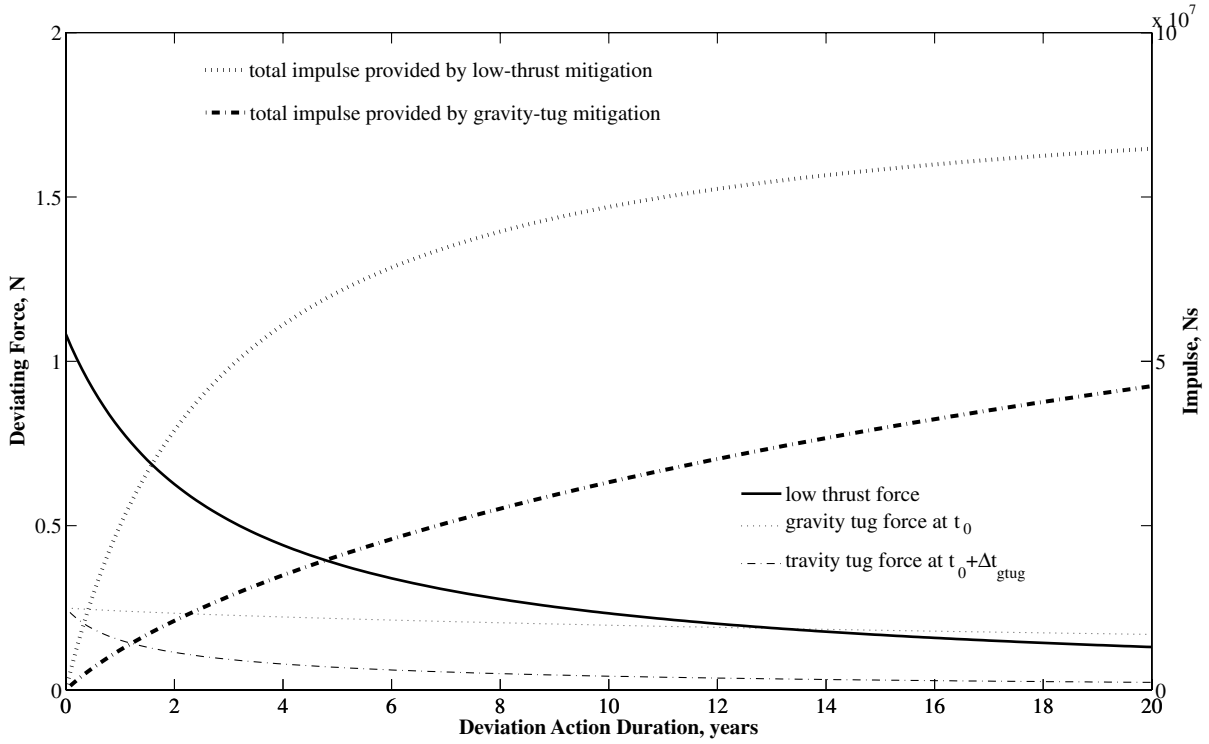

Fig. 13 Comparison between a low-thrust mitigation mission and a gravity tug for a possible deviation of Apophis. Initial mass at asteroid arrival is 5000 kg for both methods.

provided by the gravity tug becomes higher than that achieved by the low thrust.

Before concluding this section, it is worth noting that the spacecraft has to hover at a relatively close distance from the asteroid and accurately maintain its position and velocity. Because the shape and composition of the asteroid have an impact on its gravity field, the gravity tractor is not totally immune from the problems related to the unknown composition and morphology. Therefore, hovering control in a inhomogeneous gravity field generated by a nonspherical asteroid is an issue that has to be taken into account. However, a complete analysis of the effect of a nonspherical asteroid on the control of the gravity tug is out of the scope of this paper and was already performed by other authors. The interested reader can refer to the work of Broschart and Scheeres [39] and Kawaguchi et al. [40] for more details.

IV. Multicriteria Optimization Problem Formulation

The optimality of each strategy is defined here through a number of criteria or objectives that have to be attained. Unlike single-objective problems, multiple-objective problems look for a set of optimal values rather than a single optimal value. The general problem is to find a set X of feasible solutions $\mathbf{x}$ such that the property $P(\mathbf{x})$ is true for all $\mathbf{x} \in X \subseteq D$:

$$X = \{\mathbf{x} \in D | P(\mathbf{x})\} \tag{47}$$

where the domain D is a hyperrectangle defined by the upper and lower bounds on the components of the vector $\mathbf{x}$:

$$D = \left\{ x_i | x_i \in \left[b_i^l, b_i^u \right] \subseteq \Re, i = 1, \ldots, n \right\} \tag{48}$$

All of the solutions satisfying property P are defined here to be optimal with respect to P, or P-optimal, and X can be said to be a P-optimal set. In the case of multi-objective optimization, if P is a dominance condition or Pareto optimality condition for the solution $\mathbf{x}$, then the solution is Pareto-optimal if $P(\mathbf{x})$ is true.

Each function vector j is associated with a scalar dominance index I_d such that

$$I_d(\mathbf{x}_j) = |\{i | i \in N_p \wedge \mathbf{x}_i \succ \mathbf{x}_j\}| \tag{49}$$

where the symbol $\|$ is used to denote the cardinality of a set, $\succ$ represents the dominance of the $\mathbf{x}_i$ solution over the $\mathbf{x_j}$ solution, and N_p is the set of the indices of all of the available feasible solutions. A solution vector $\mathbf{x}_i$ dominates a solution vector $\mathbf{x}_j$ when all of the components of the criteria, or objectives, vector $\mathbf{f}(\mathbf{x_i})$ associated with $\mathbf{x_i}$ are better (higher or lower) than all of the components of the criteria vector $\mathbf{f}(\mathbf{x}_j)$ associated with $\mathbf{x}_j$. The property $P(\mathbf{x})$ in this case simply defines nondominated solutions:

$$X = \{\mathbf{x} \in D | I_d(\mathbf{x}) = 0\} \tag{50}$$

The search for the P-optimal sets X for each strategy was performed through an agent-based search approach hybridized with a domain decomposition technique [41,42].

Three criteria, or figures of merit, were selected to define the optimality of each strategy:

1) The warning time $t_w = t_{\text{MOID}} - t_l$ is the interval between the launch date and the time at the point of closest approach. This figure of merit defines how far in advance we need to know that an impact is going to occur; it gives a measure of our capability of quickly reacting to an incoming danger.

2) The mass into space m_0 at departure is the mass of the spacecraft at the Earth after launch. This figure of merit gives a measure of how difficult implementing a given strategy could be; if m_0 is not within our launch capabilities, the difficulty of a given strategy increases.

3) The total deviation Δr_{tot} at encounter is calculated as $\Delta r_{\text{tot}} = \|\Delta \mathbf{r} + \delta \mathbf{r}\|$, where $\Delta \mathbf{r}$ is the vector distance of the asteroid from the Earth at the MOID point and $\delta \mathbf{r}$ is the variation given by the integration of Gauss's planetary equations [see Eq. (2)]. This figure of merit, together with the mass into space, gives a measure of how easy it is to deflect an asteroid with a given method. Note that we use the total deviation as figure of merit and not the ability of a particular deflection method to avoid the passage of the asteroid through dangerous keyholes [43]. In this case, even small $\delta \mathbf{r}$ would produce significant results, greatly enhancing the effectiveness of given deflection method.

Table 3 Design margins for the spacecraft mass

Strategies	m_0 margin
Solar collector	25%
Electric propulsion	25%
Mass driver	25%
Gravity tug	25%
Nuclear interceptor	10%
Kinetic impactor	5%

The t_{MOID} is the date at which the asteroid reaches the minimum orbit interception distance point from the Earth. Note that the Earth is not necessarily at that physical point in the orbit; the aim of this analysis is to measure the effectiveness and efficiency of each deviation method and not to reproduce a real impact scenario. In the following analyses, the t_{MOID} for each asteroid is the same for all of the deflection strategies and is kept fixed for all of the simulations.

Even though the strategies were modeled with a very conservative approach, an additional margin on the mass into space m_0 was added to take into account the corrective maneuvers required during both the transfer leg and the deflecting arc. These margins, which can be found in Table 3, are also related, to some extent, to the maturity level of a given technology.

The criteria vector for a given method A is then defined as

$$\mathbf{f}^A = \left[t_w^A, m_0^A, -\left\| \Delta r + \delta r \right\|^A \right]^T \tag{51}$$

where m_0 is augmented according to the design margin for method A. The problem is to find the set X of feasible solutions that are not dominated with respect to the criteria vector $\mathbf{f}^A$. Each solution corresponds to a mission leaving the Earth at a departure time t_0, performing a transfer to the asteroid either along a Lambert's arc or a low-thrust spiral for a transfer time T, and then applying the deviation action for a time t_{push}. For deviation strategies for which the action is impulsive, such as kinetic impactor and nuclear interceptor, the transfer was modeled as a simple Lambert's arc. The velocity change at the Earth required to reach the asteroid was used to compute the propellant mass. For all of the other deviation strategies, the transfer was modeled as a low-thrust spiral through a shape-based approach [44], assuming a departure from the Earth with zero relative velocity. The time t_{push} was set to be equal to the difference between the time at the point of closest approach and the time at interception, except for those strategies for which the model is providing an optimal value for t_{push}. All celestial bodies are considered to be point masses with no gravity, and analytical ephemerides are used for the Earth and the asteroids. The general solution vector is defined as

$$\mathbf{x} = [m_0, t_0, T, n_R, \lambda_{s1}, \lambda_{s2}]^T \tag{52}$$

where n_R is the number of revolutions of the Lambert's arc or of the low-thrust spiral, and λ_{s1} and λ_{s2} are two shaping parameters for the low-thrust arcs. The search domain D is defined by the values in Table 4; therefore, for each deflection method, we looked for all of the mission opportunities with a launch in the interval of $t_{\text{MOID}} - 1000$ to $t_{\text{MOID}} - 7300$ MJD2000 (i.e., modified Julian days since 1 January 2000 at 1200 hrs) and a transfer time in the interval of 25–1000 days. Note that the range of masses into space is pretty wide to account for a large variety of spacecraft designs, from microsatellites to multiton spacecraft. Note that the propellant mass required for the transfer is subtracted from m_0 when the spacecraft is at the asteroid. The residual mass (either m_i or m_d, depending on the model) is then used to compute the deviation. All of the missions that had a residual mass low enough to produce a deviation close to zero were discarded and were not included in the Pareto sets.

Table 4 Search domain for the multi-objective analysis

m_0	t_0	T	n_R	λ_{s1}	λ_{s2}
100	$t_{\text{MOID}} - 7300$	25	0	−1	−1
100,000	$t_{\text{MOID}} - 1000$	1000	3	1	1

V. Results

A preliminary analysis was performed on the asteroid Apophis because of the potential impact with the Earth in 2036. Figure 14 shows the Pareto-optimal solutions found by the agent-based search for each one of the deviation methods. Each solution shown in Fig. 14, each black dot, represents a Pareto-optimal deviation mission to the asteroid Apophis, which means that no other mission can be designed by changing the parameters in the solution vector in Eq. (52) that improves all three criteria at the same time.

Note that the range of warning times and mass into space are almost the same for all six methods, whereas the range of the achieved deviation is substantially different. For example, for the same mass into space and for the same warning time, the solar collector and nuclear interceptor are achieving a deviation that is 2 orders of magnitude higher than the kinetic impactor. Furthermore, all strategies that employ a single-impulse transfer present a characteristic striped distribution of the solutions, mainly due to the periodicity of the optimal launch date. The direction of application of the deviating action, in fact, depends solely on the transfer, and therefore an optimal launch date corresponds to a Pareto-optimal solution.

The surfaces plotted in Figs. 14a, 14c, and 14d have a plateau at a deviation value of about 400,000 km. The plateau is due to the fact that the integration was stopped once the deviation reached one Earth–moon distance. For the hypotheses behind the proximal motion equations to hold true, the variation of the orbit radius δr must be small compared with the unperturbed orbit. Therefore, the Earth–moon distance was taken as the upper threshold limit, because this is considered to be sufficient to ward off the threat of an impact. The size of the plateau regions already suggests that both the solar collector and nuclear interceptor provide similar performances. Note that the two approaches are utterly different, as the deviation is achieved through a continuous thrusting arc in the former case and through an impulsive change of the linear momentum in the latter.

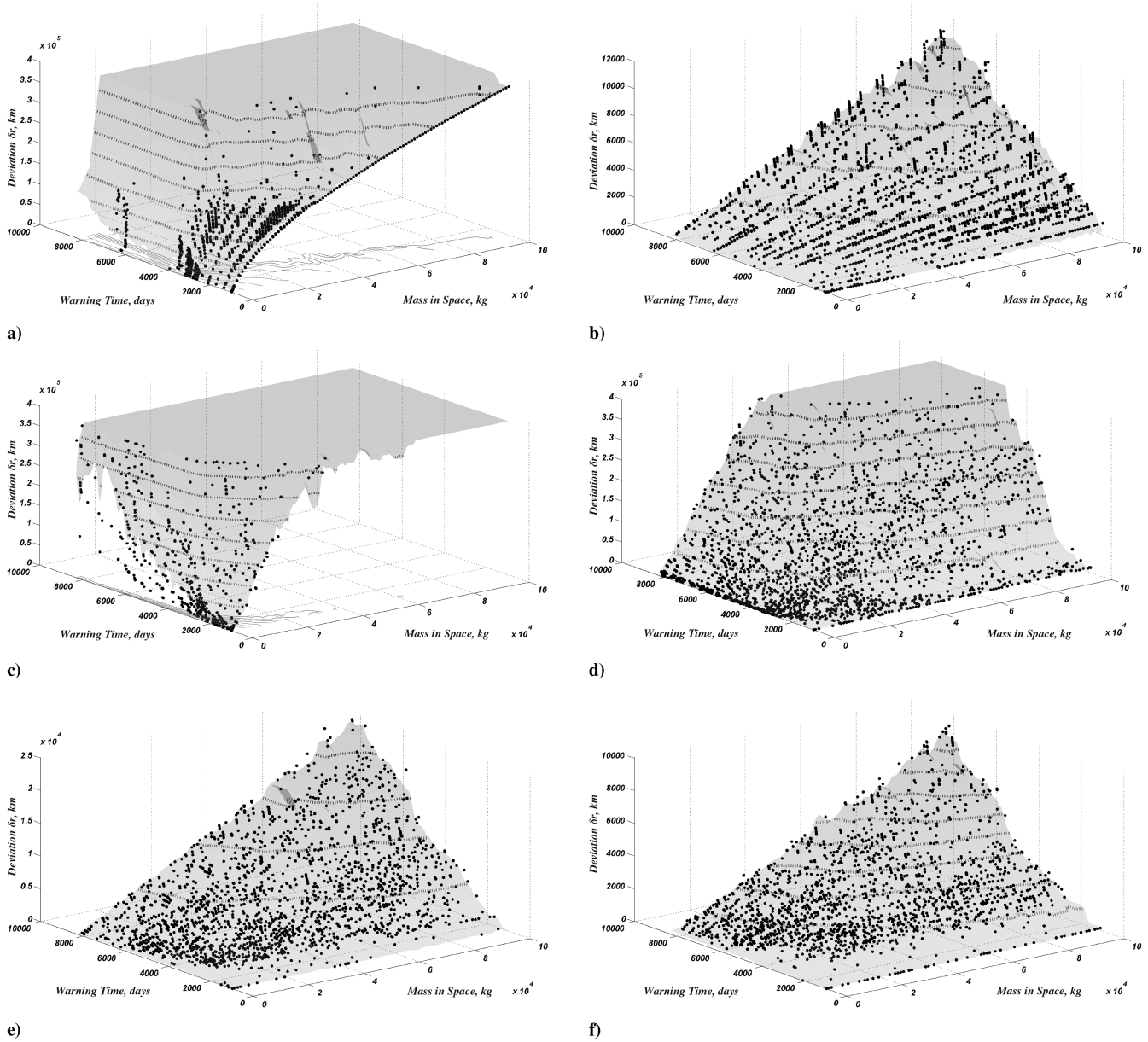

Fig. 14 Pareto sets for the six deviation methods applied to asteroid Apophis: a) nuclear interceptor, b) kinetic impactor, c) solar collector, d) mass driver, e) low-thrust propulsion, and f) gravity tug.

Table 5 Keplerian elements of the asteroids used in this study

	a, AU	e	i, deg	Ω, deg	ω, deg	M, deg	Epoch, MJD	t_{MOID}, MJD
Apophis	0.922	0.191	3.331	204.5	126.4	222.3	53800.5	62564.0
Aten case	0.875	0.313	7.828	259.9	50.65	97.21	62481.0	62481.0
Apollo case	1.706	0.518	10.70	266.8	121.2	18.09	62488.0	62488.0

Table 6 Some physical characteristics of the asteroids used in this study and the approximated impact frequency

	M_a, kg	Density, kg/m^3	Diameter, m	Estimated impact frequency	Rotation, h
Apophis	4.6×10^{10}	2500	328	1 every 100,000 years	30.54
Aten-1	5.0×10^{8}	2500	73	1 every 1000 years	4.33
Aten-2	5.0×10^{9}	2500	156	1 every 10,000 years	4.33
Aten-3	5.0×10^{10}	2500	337	1 every 100,000 years	4.33
Aten-4	5.0×10^{11}	2500	726	1 every 1,000,000 years	4.33
Apollo-1	5.0×10^{8}	2500	73	1 every 1000 years	4.33
Apollo-2	5.0×10^{9}	2500	156	1 every 10,000 years	4.33
Apollo-3	5.0×10^{10}	2500	337	1 every 100,000 years	4.33
Apollo-4	5.0×10^{11}	2500	726	1 every 1,000,000 years	4.33

A. Selected Asteroids

Although Apophis is an interesting study case, due to the threat that it poses to the Earth, additional case studies were considered to add comprehensiveness to this work. Instead of selecting more specific asteroids, it was decided to use the mean semimajor axis, eccentricity, and inclination of two sets of 100 asteroids belonging to the Aten and Apollo groups. The asteroids in the sets were taken from the list of the most dangerous Earth-crossing asteroids in NASA's NEO program database.[††] The angular Keplerian elements Ω, ω, and M_0 were modified such that the MOID for a fixed collision date was minimal. Table 5 shows the Keplerian elements and t_{MOID} used in this study for Apophis and for the two additional virtual asteroids.

Apophis is assumed to have a mass of 4.6×10^{10} kg, which is equivalent to an asteroid with a diameter of 328 m if a density of 2500 kg/m^3 and spherical shape are considered. The impact frequency of an object of this size is approximately 1 every 100,000 years [1]. For the Aten and the Apollo cases, we considered masses ranging from 5.0×10^{8} to 5.0×10^{11} kg (see Table 6 for a complete list of the cases analyzed in this paper).

B. Pareto Contour Lines

A simple way to compare the 3-D Pareto fronts of the different strategies and asteroids is by plotting deviation isolines. Figure 14 shows the isolines for a deviation of 13,720 km for each deviation strategy and each case studied. This deviation was calculated taking into account the deflection of the trajectory of Apophis due to the gravity attraction of the Earth at its final approach and correcting a distance of 1 Earth radius with a hyperbolic factor that depends on the relative velocity between the Earth and the threatening object [4]. The deflection isoline of 13,720 km is used in all of the plots in Fig. 14 to facilitate the comparison between the different asteroids, despite the fact that the hyperbolic corrected distance would be lower for our Aten and Apollo cases, because the relative velocities of those at encounter with the Earth are higher than the Apophis relative velocity and should therefore be less affected by the Earth gravity.

In the three cases with mass of the order of 5×10^{10} kg (i.e., Apophis, Aten-3, and Apollo-3) only three strategies (namely, the mass driver, the nuclear interceptor, and the solar collector) yield the desired deviation with a mass in space smaller than 100,000 kg and a warning time shorter than 10 years. The low-thrust method is also able to provide 13,720 km deflection, but only with a mass in space close to 100,000 kg and 20 years of warning time.

The kinetic impactor is remarkably close to the low thrust in the Aten cases (Figs. 15b and 15c), especially for short warning times; in the Apollo cases (Figs. 15f–15h), it not only clearly outperforms the low-thrust strategy, but its efficiency increases almost tenfold when compared with the Aten case. The main reason for this high efficiency of the kinetic impactor in the Apollo cases is because Apollo's asteroid had higher eccentricity and inclination and thus higher relative velocity with respect to the orbit of the Earth, and a high-speed impact is less expensive, in terms of propellant mass, than in the Aten cases and more mass-efficient than a rendezvous.

Note that for small asteroids (Figs. 15b, 15c, 15f, and 15g), simple methods such as the kinetic impactor are able to provide the required deviation with a relatively small mass in space. On the other hand, for larger asteroids (Figs. 15e and 15i), only the three more efficient methods are able to provide the required deviation within the given range of mass into space and warning time.

C. Strategy Comparison

The effectiveness and efficiency of each strategy are expressed through a set of Pareto-optimal points (e.g., Fig. 14). To compare one strategy with the others, it is possible to use the concept of dominance of one Pareto set over another: an element (or solution belonging to the Pareto set) i of strategy A is said to be dominated by element j of strategy B if all of the components of the vector objective function $\mathbf{f}_j^B$ are better (i.e., t_w and m_0 are smaller and $\|\Delta r + \delta r\|$ is bigger) than all of the components of the vector objective function $\mathbf{f}_i^A$. Then the dominance index $I_i(m_A)$ of an element i of strategy A with respect to strategy B is the cardinality of the set of elements of the Pareto-optimal set of strategy B that dominates element i:

$$I_i(m_A) = \left| \left\{ j \middle| \mathbf{f}_i^A \prec \mathbf{f}_j^B \right\} \right| \tag{53}$$

where the dominance symbol $\prec$ in Eq. (53) means that $\mathbf{f}_j^B$ dominates $\mathbf{f}_i^A$ (i.e., all of the components of $\mathbf{f}_j^B$ are better than all of the components of $\mathbf{f}_i^A$). Thus, if the value of the dominance index of the element i is 0, it means that there is no solution in the Pareto-optimal set of strategy B that has all three criteria that are better than the three criteria associated with element i. We can now say that strategy A dominates strategy B if the percentage of the elements of A that are dominated by B [i.e., the percentage of elements of A with dominance index $I(m_A)$ different from 0] is less than that of the elements of B that are dominated by A:

$$d_i(m_A) = \begin{cases} 1 & \text{if } I_i(m_A) > 0 \\ 0 & \text{if } I_i(m_A) = 0 \end{cases}$$
$$m_A \succ m_B \Rightarrow \frac{1}{N_A} \sum_{i=1}^{N_A} d_i(m_A) < \frac{1}{N_B} \sum_{j=1}^{N_B} d_j(m_B) \tag{54}$$

[††]Data available online at http://neo.jpl.nasa.gov/ [retrieved 16 October 2008].

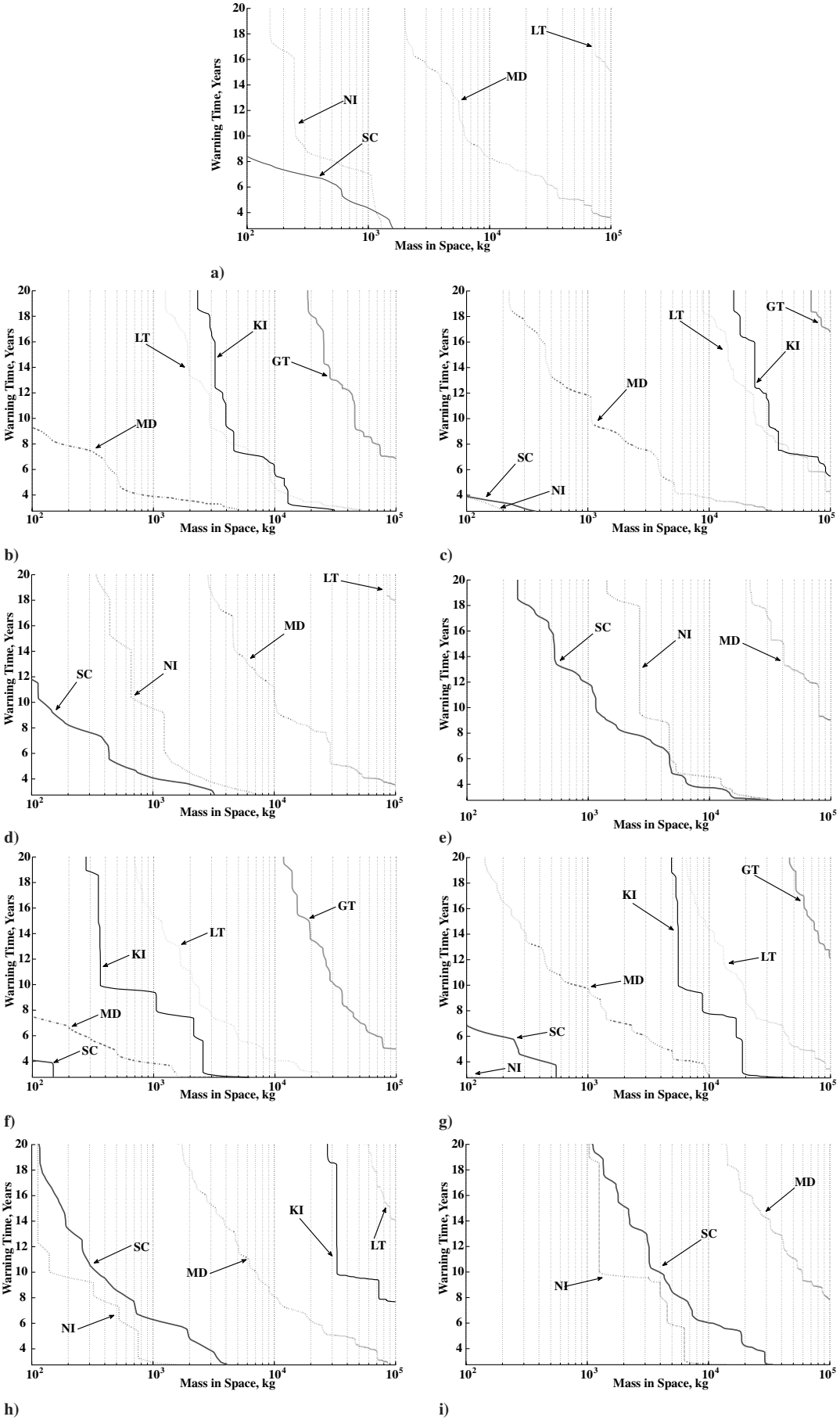

Fig. 15 Pareto front contour lines for a deviation of 13,720 km for all of the analyzed deviation methods [solar collector (SC), low thrust (LT), mass driver (MD), nuclear interceptor (NI), kinetic impactor (KI), gravity tug (GT)]; each figure is for a different mass of the asteroid: a) Apophis case, b) Aten-1 case, c) Aten-2 case, d) Aten-3 case, e) Aten-4 case, f) Apollo-1 case, g) Apollo-2 case, h) Apollo-3 case, and i) Apollo-4 case.

where N_A is the total number of the solutions in the Pareto set of method (or strategy) m_A, and N_B is the total number of solutions in the Pareto set of method (or strategy) m_B.

Tables 7–9 show the dominance of the different strategies applied to Apophis, Aten-3, and Apollo-3 (i.e., three cases with similar mass). The numbers in the tables are the percentage of elements of the method in the corresponding row that dominate over the elements of the method in the corresponding column. For example, if we look at Table 7, 100% of the solutions in the Pareto set of the mass driver dominate (i.e., all three criteria are better) the solutions in the Pareto set of the low thrust. Note that the numbers in every column do not add up to 100 with the corresponding numbers in every row. For example, for Apophis (see Table 7), 14% of the kinetic impactor solutions are dominant over low-thrust solutions, whereas 98% of low-thrust solutions are dominant over kinetic impactor solutions. The reason for that is that we compute the percentage of points within each Pareto set; therefore, it could well be that 100% of the points of a set are dominating only a small fraction of the points of another set.

From the dominance comparison, the solar collector and nuclear interceptor prove to be the dominant methods in the studied domain. The solar collector achieves better performance than the nuclear interceptor for the Atens class, but not for the Apollo class. This is due mainly to the fact that the smaller semimajor axis of the Atens group means better solar radiation and therefore higher efficiency of the solar collector. It is interesting to note that the kinetic impactor dominates the low-thrust option for the Apollo case. The same result can be seen in Fig. 15, though limited to one particular value of deflection δr.

Although, as shown in Fig. 15, techniques such as kinetic impactor and gravity tug are effective for small-size asteroids, the relative performance difference between two deflection strategies does not change; therefore, we report only three sample tables for the dominance evaluation. Furthermore, it should be noted that due to the stochastic nature of the search for Pareto-optimal solutions performed by the optimizer, the curves in Fig. 15 can locally change if the optimizer is run several times. As a consequence, the dominance evaluation is also subject to minor changes (few percentage points).

VI. Influence of the Technology Readiness Level

As an additional criterion, we considered the technology readiness level (TRL) of each method as a measure of its expected viability in the near future. In the case of an impact, we assumed that the required time to implement a given deviation method had to take into account the necessary development effort and that the development effort was driven by the piece of technology, composing the deviation method, with the lowest TRL. In the following, the development effort will be measured in man-years (amount of work performed by an average worker in 1 year). Although this is not an exact measure of the time required to implement a given technology, it gives a good estimation of the added difficulty to bring a given technology to full operation capability. The actual development time depends on the amount of available resources and on political considerations that are out of the scope of this paper. Therefore, we assume that the development effort is a measure of the required delay in the implementation of a given deflection method. To be more precise, the warning time is redefined to be the time between the point when a given technology starts to be developed and the predicted impact time. For example, given a technology, we need a man-time Δt_{dev} to bring that technology to a sufficient level of development to be launched; therefore, the warning time becomes $t_w = t_{\text{MOID}} - t_l + \Delta t_{\text{dev}}$.

We use a standard definition of TRL [45,46], as summarized in Table 10. We assume no limitations due to economic or political issues and no developments driven by other applications or breakthrough discoveries. Therefore, we assign the current TRL to each of the deviation methods and we assume that the TRL will remain constant till $t_{\text{MOID}} - t_w$. These assumptions correspond to a situation in which cost is not an issue in case a global threat has to be faced, but on the other hand, both economic and political issues prevent any development not motivated by a confirmed impact.

Table 7 Strategy dominance for Apophis

	Solar collector	Low thrust	Mass driver	Nuclear interceptor	Kinetic impactor	Gravity tug
Solar collector	——	100	100	95	100	100
Low thrust	0	——	0	0	98	100
Mass driver	0	100	——	0	100	100
Nuclear interceptor	5	100	100	——	100	100
Kinetic impactor	0	14	0	0	——	100
Gravity tug	0	0	0	0	2	——

Table 8 Strategy dominance for Aten-3

	Solar collector	Low thrust	Mass driver	Nuclear interceptor	Kinetic impactor	Gravity tug
Solar collector	——	100	100	95	100	100
Low thrust	0	——	0	0	88	100
Mass driver	0	100	——	0	100	100
Nuclear interceptor	8	100	100	——	100	100
Kinetic impactor	0	42	0	0	——	100
Gravity tug	0	0	0	0	1	——

Table 9 Strategy dominance for Apollo-3

	Solar collector	Low thrust	Mass driver	Nuclear interceptor	Kinetic impactor	Gravity tug
Solar collector	——	100	100	14	100	100
Low thrust	0	——	0	0	0	100
Mass driver	0	100	——	0	100	100
Nuclear interceptor	97	100	100	——	100	100
Kinetic impactor	0	100	0	0	——	100
Gravity tug	0	0	0	0	0	——

Table 10 Technology readiness levels

TRL	Technology readiness
1	Basic principles observed and reported
2	Technology concept and/or application formulated
3	Analytical and experimental critical function and/or characteristic proof-of-concept
4	Component and/or breadboard validation in laboratory environment
5	Component and/or breadboard validation in relevant environment
6	System/subsystem model or prototype demonstration in a relevant environment (ground or space)
7	System prototype demonstration in a space environment
8	Actual system completed and flight-qualified through test and demonstration (ground or space)
9	Actual system flight-proven through successful mission operations

The TRL of each deviation methodology was determined taking into account past missions and scientific research to date. The TRL for each method was mapped into the number of man-years Δt_{dev} for increasing a given technology from the current TRL to TRL 9 through the logistic function

$$t_{\text{dev}} = \frac{a}{1 + e^{-\frac{\Lambda - t_c}{\tau}}} + b \tag{55}$$

where t_{dev} is the required development effort (measured in man-years) to bring a technology from TRL 1 to TRL Λ. The parameter t_c represents a turning point for the development of a technology when the critical function characteristics have already been demonstrated experimentally and analytically but the components have not yet been tested in a relevant environment. Around that point, we expect a maximum increase in the investments to turn a conceptual design into a first hardware prototype. In the following, we set $t_c = 5$, which is a value corresponding to TRL 5. The coefficients a, b, and t were chosen so that

$$\begin{gathered} t_{\text{dev}}(\Lambda = 2) = 0 \qquad t_{\text{dev}}(\Lambda = 9) = 15 \\ t_{\text{dev}}(\Lambda = 7) - t_{\text{dev}}(\Lambda = 4) = 10 \end{gathered} \tag{56}$$

The set of boundary conditions in Eq. (56) corresponds to a maximum development effort of 15 man-years from TRLs 2 to 9 and a development effort from breadboard to first prototype system demonstration into space of 10 man-years. The resulting Δt_{dev} is simply the difference between the t_{dev} at TRL 9 and the t_{dev} at a given TRL Λ (see Fig. 16).

Note that we start with a minimum TRL of 2, because the basic concept and the application have been already formulated for all of the deflection methods. In the assignment of TRL to each deflection method, we will then distinguish between innovate technologies before or during the mission-assessment phase (TRLs 1 to 4) and existing technologies during mission-definition phase (TRLs 5 to 9).

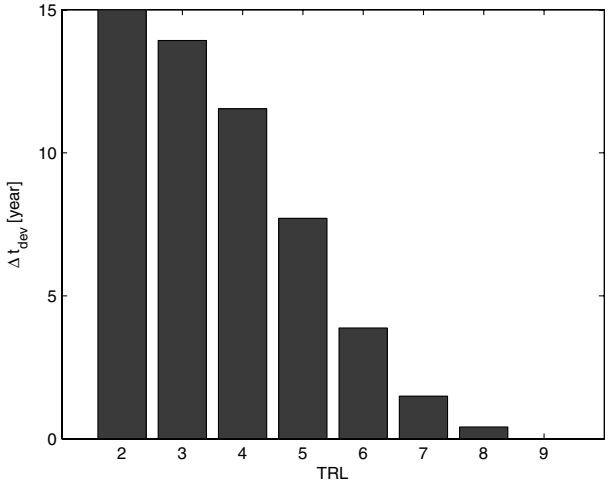

Fig. 16 TRL mapping into required development effort to reach full operational capabilities.

In the following, we assign a TRL to each of the deflection methods. Each deviation method is characterized by a number of critical technologies that need to be developed to make the method actually feasible. The technologies considered in this analysis are only strictly related to each preceding model of deflection method and do not include the development of new launch capabilities and the required increase in the knowledge of the physical and orbital characteristics of the asteroids. Once the critical technologies are identified and a TRL is assigned to each of them, we assign the TRL of the least developed technology to the whole deflection method. Because the TRL for some methods is uncertain due to several concurrent factors, we assign an interval of TRLs to each deflection method. These intervals represent our level of confidence in the present level of development of a given technology. The assignment is based on Table 10 and on the assumption that a technology at TRL 9 that is reused in a new application with new requirements needs to be downgraded to TRL 4.

A. Kinetic Impactor

Although the kinetic impactor strategy has not been completely proven yet, a mission with similar characteristics, Deep Impact, was already successfully flown. Furthermore, although the impact velocity is a critical issue for this strategy, the average impact velocity of all solutions found in this study was 10 km/s, which is indeed very similar to the Deep Impact crash velocity ($\sim$10.2 km/s). For this deflection method, we consider two critical issues: high-precision targeting and enhancement factor. The former issue would require a better knowledge of the motion of the center of mass and rotational state of the asteroid to correctly hit the asteroid and transfer the required Δv; the latter issue would require a better knowledge of the composition and morphology of the asteroid. Thus, both cases are related to an increased knowledge of the characteristics of the asteroid. The former issue would also require the development of accurate navigation and orbit-determination capabilities for fast, close encounters. However, we can assume that this technology is already available and at TRL 9, given all of the past and present missions using gravity-assist maneuvers. Because only one example of high-velocity impact exists, we assign a TRL ranging between 7 and 8 to the kinetic impactor.

B. Nuclear Interceptor

Nuclear weapons have not been tested in space because the Limited Test Ban Treaty forbids all nuclear use in both space and atmosphere. Furthermore, although the effects of a nuclear explosion can be considered to be well known, there has not been any nuclear interceptor prototype or any equivalent prototype in space; therefore, the TRL should be no higher than 6. On the other hand, the launch of a nuclear warhead is fully developed; thus, we assign a TRL ranging from 6 to 8.

C. Low Thrust

Low thrust requires the following main critical technologies: low-thrust propulsion, nuclear power generation, autonomous rendezvous and landing, and an anchoring system. Low-thrust engines delivering the required level of thrust have been used as main propulsion systems since 1998 with Deep Space 1; therefore, they

can be considered to already be at TRL 8. On the other hand, some missions in the Pareto set require a thrusting time of more than 1000 days, which exceeds the operational lifetime of current electric engines. For those missions, either a complete redesign of the propulsion system or multiple engines would be required; in the former case, the TRL would be not higher than 4. Rendezvous and landing operations for small spacecraft can be considered at TRL 7 due to previous and ongoing missions to comets and asteroids (such as Rosetta [47] and Hayabusa [40]). Nuclear reactors delivering between 1 to 10 k have already flown since 1965 (e.g., the U.S. SNAP-10A), and higher-power reactors can be derived from terrestrial reactors with limited new developments; thus, this technology can be considered to be between TRLs 6 and 7. An anchoring system was already designed for the lander of Rosetta, though for more massive spacecraft, the anchoring and landing system would require further development; therefore, their TRL cannot be considered to be higher than 6. Overall, the TRL for the low-thrust method can be considered to range from 4 to 6.

D. Gravity Tug

Gravity tug requires the following main critical technologies: autonomous proximal motion control in an inhomogeneous gravity field, nuclear power generation, and low-thrust propulsion. A hovering approach to the asteroid Itokawa was used by the mission Hayabusa, and the same technique is proposed for the gravitational tug, but to a completely different level of accuracy and autonomy; therefore, its TRL should be between 3 (no test in relevant environment) and 5 (if Hayabusa is considered to be an example of hovering in relevant environment). Low-thrust propulsion has the same TRL as for low-thrust deviation methods and shares the same issues (in particular, the operational lifetime, because the number of missions with a pushing time higher than 1000 days is higher than for the low thrust). Nuclear power generation for this method has the same TRL as for the low-thrust technique; therefore, the overall TRL for the gravity tug ranges from 3 to 5.

E. Mass Driver

Mass driver requires the following main critical technologies: autonomous rendezvous and landing, autonomous mining in microgravity, high-power rail gun system, nuclear power generation, and an anchoring system. Magnetic rail gun systems have already been developed and used on Earth for other applications [29]; therefore, we can assume a TRL 5 for this technology. Following the same arguments given for the low-thrust method, both rendezvous and landing and nuclear power technologies should be at TRL 7. The anchoring system and the mining system in microgravity instead require a substantial development [31,32,48,49]; thus, their TRL is no higher than 4. Though drilling systems have been already tested in space, the level of power involved in a successful implementation of the mass driver would require a substantial redesign of the mining and anchoring system to cope with the microgravity conditions. Because a conceptual design for this technology already exists (TRL 2) [17], we can assign a TRL ranging between 2 and 4 to the mass driver.

F. Solar Collector

Solar collector requires the following main critical technologies: adaptive optics, deployment and control of ultralight mirrors, autonomous orbit control, and accurate autonomous pointing. The mirrors have to focus the light of the sun in every operational conditions; therefore, the curvature has to be actively controlled. Furthermore, it is expected that the light is collimated by a series of lenses. The collimation of the beams is of primary importance to maintain the required power density, especially for rotating asteroids with high elongation, for which the closest and farthest distance from the spacecraft could be considerable. Adaptive optics for terrestrial [50] and space applications have been developed and used in space on telescopes; therefore, their TRL could be 7. On the other hand, it is required to have an autonomous control of the pointing and of the focusing dependent on the power density of the illuminated spot. This would require a substantial redesign and a new development; therefore, the TRL is between 2 and 3. The deployment of ultralight structures of small to medium dimensions has already been tested in space and would be between TRLs 6 and 7 [51], and ultralight adaptive mirrors for space have already been developed and prototyped and would be between TRLs 4 and 5 [52,53]. On the other hand, the deployment and control of large focusing mirrors is still at a conceptual stage and therefore at TRL 2. Accurate autonomous orbit control is at the same level of the gravity tug and is therefore at TRL 4. The overall TRL for the solar collector is between 2 and 3.

Table 11 TRL for all deviation methods

Deviation method	TRL intervals
Kinetic impactor	7–8
Nuclear interceptor	6–8
Low thrust	4–6
Gravity tug	3–5
Mass driver	2–4
Solar concentrator	2–3

The TRL intervals for each deviation methods are summarized in Table 11 and were translated into a Δt_{dev} according to Fig. 16. The development time due to the technology readiness level is applied to the Pareto-optimal sets by extending the warning time t_w:

$$\mathbf{f} = [t_w + \Delta t_{\text{dev}}, m_0, -\|\Delta r + \delta r\|]^T \tag{57}$$

Because the impact date is kept fixed for all of the strategies, all of the Pareto-optimal solutions that would require a warning time (such that the arrival date at the asteroid exceeds the t_{MOID}) are removed from the comparison. As a consequence, a strategy with a low technology readiness would require a longer warning time for the same deviation or a lower deviation for the same warning time. Table 12 shows the intervals of dominance of all of the strategies for a simulated deviation of Apophis after applying the range of TRL from Table 11.

By comparing Table 12 with Table 7, few preliminary considerations can be drawn. The first is that when the technology readiness level is considered, the kinetic impactor becomes competitive because its Pareto front encloses parts of the criteria space that the other strategies are not able to cover. On the other hand, even after the technology readiness shifting is applied, the solar collector strategy remains particularly competitive, despite the fact that the nuclear interceptor has better comparative performance in this table (only between 6 and 17% of the domain is still dominated by the solar collector method). Also note that the solar collector, along with all of the other nonimpulsive deviation techniques, does not present a risk of fragmentation and offers the possibility to

Table 12 Apophis TRL comparison table ($a = 0.92$ AU)

	Solar collector	Low thrust	Mass driver	Nuclear interceptor	Kinetic impactor	Gravity tug
Solar collector	——	100	100	6–17	100	100
Low thrust	9–52	——	9–39	0	0–86	100
Mass driver	0–22	99–100	——	0	99	99–100
Nuclear interceptor	100	100	100	——	100	100
Kinetic impactor	76–68	100–45	79–63	10–0	——	100
Gravity tug	25–22	1–0	25–5	0	0	——

accurately control the deviation action. For example, considering an energy density limit of 1 J/g [25] as a first approximation, a nuclear interceptor with a yield of 5 kton or more would probably cause a fragmentation of an Apophis-size, or smaller, asteroid. This aspect definitively deserves a further investigation to better understand the consequences of a possible fragmentation for small- to medium-size asteroids.

VII. Conclusions

In this paper, a comparison of six different deflection strategies was presented: nuclear interceptor, solar collector, mass driver, low-thrust propulsion, gravity tug, and kinetic impactor. The comparison was based on four different criteria that translate quantitatively from a number of qualitative statements defining the performance of a particular deviation strategy: ease of deflection, cost of the mission, complexity of the approach, readiness of the deviation strategy, and response time.

The results from this study show that the solar collector and the nuclear interceptor options achieve the best results in terms of deviation, mass into space, and warning time. The nuclear interceptor is better than the solar collector in the Apollo case and in the Apophis case after the application of the technology readiness shift in the warning time. On the other hand, the solar collector solutions dominate the nuclear interceptor in both the Apophis and Aten cases if no technology readiness shift is applied. Furthermore, it should be noted that despite the low technology readiness, the solar collector still remains competitive against most of the deflection methods.

Kinetic impactor and low thrust display comparable performance, and both prove to be interesting alternatives for deviating asteroids with a mass below 10^{10} kg, particularly the kinetic impactor, if the technology level is considered. Kinetic impactor performance is better for the Apollo class of asteroids, especially for short warning times, whereas low thrust dominates in the Aten category, especially for long warning times.

The mass driver presents an intermediate performance between the two pairs: solar collector with nuclear interceptor and kinetic impactor with low thrust, although its technology readiness is still considerably low compared with the kinetic impactor, and its performance is not as good as solar collector. Note that the estimation of the technology readiness of each deviation method is subject to the current and future political and economical situations. Therefore, a complete evaluation of the methods presented in this paper would also require considering the economical and political aspects in the development of a specific technology, which was not done in this analysis.

On the other hand, the comparison methodology proposed in this paper, based on the concept of set dominance, allowed us to compare two or more methods using sets of hundreds of solutions, each one representing a complete mission with a specific launch date and transfer time, instead of using a single typical or hypothetical mission case. Therefore, the comparison is not subject to any particular ideal or fictitious scenario in which the deflection method is applied, and it takes into account the fact that for some methods, some mission opportunities could be prohibitive or not feasible. Though we use only three quantitative criteria in this paper, the same procedure could be extended to a more extensive analysis, including more figures of merit.

Finally, though the results in this paper cannot be used to rule out any of the analyzed deflection methods, they suggest some promising directions of research in which the performance of a particular method is high but the technology readiness is still low.

Acknowledgments

The authors would like to thank Marco Guglielmi, Head of the Technology Strategy Section of ESA, for the precious advice on the definition of the logistic function for the technology readiness level mapping into a development effort.

References

[1] Stokes, G. H., and Yeomans, D. K., "Study to Determine the Feasibility of Extending the Search for Near-Earth Objects to Smaller Limiting Diameters," NASA, Aug. 2003.

[2] "Near-Earth Objects Survey and Deflection Analysis of Alternatives," NASA, Mar. 2007.

[3] Izzo, D., "On the Deflection of Potentially Hazardous Objects," 15th AAS/AIAA Space Flight Mechanics Conference, Copper Mountain, CO, American Astronautical Society Paper 05-141, Jan. 2005.

[4] Scheeres, D. J., and Schweickart, R. L., "The Mechanics of Moving Asteroids," AIAA Planetary Defense Conference, Orange County, CA, AIAA Paper 2004-1446, Feb. 2004.

[5] Carusi, A., Valsecchi, G. B., D'abramo, G., and Bottini, A., "Deflecting NEOs in Route of Collision with the Earth," *Icarus*, Vol. 159, No. 2, 2002, pp. 417–422. doi:10.1006/icar.2002.6906

[6] Conway, B. A., "Near-Optimal Defection of Earth-Approaching Asteroids," *Journal of Guidance, Control, and Dynamics*, Vol. 24, No. 5, 2001, pp. 1035–1037. doi:10.2514/2.4814

[7] Park, S. Y., and Ross, I. M., "Two-Body Optimization for Deflecting Earth-Crossing Asteroids," *Journal of Guidance, Control, and Dynamics*, Vol. 22, No. 3, 1999, pp. 415–420. doi:10.2514/2.4413

[8] Ross, I. M., Park, S. Y., and Porter S. D. V., "Gravitational Effects of Earth in Optimizing DV for Deflecting Earth-Crossing Asteroids," *Journal of Spacecraft and Rockets*, Vol. 38, No. 5, 2001, pp. 759–764. doi:10.2514/2.3743

[9] Hall, C. D., and Ross, I. M., "Dynamics and Control Problems in the Deflection of Near-Earth Object," *Advances in the Astronautical Sciences*, Vol. 67, No. 640, 1997, pp. 1–18.

[10] *Project Icarus*, MIT Press, Cambridge, MA, 1968.

[11] Tedeschi, W. J., Remo, J. L., Schulze, J. F., and Young, R. P., "Experimental Hypervelocity Impact Effects on Simulated Planet-esimal Materials," *International Journal of Impact Engineering*, Vol. 17, Nos. 4–6, 1995, pp. 837–848. doi:10.1016/0734-743X(95)99904-6

[12] McInnes, C., "Deflection of Near-Earth Asteroids by Kinetic Energy Impacts from Retrograde Orbits," *Planetary and Space Science*, Vol. 52, No. 7, 2004, pp. 587–590. doi:10.1016/j.pss.2003.12.010

[13] Smith, P. L., Barrera, M. J., Campbell, E. T., Fedman, K. A., Peterson, G. E., and Smit, G. N., "Deflecting a Near Earth Object with Today's Space Technology," AIAA Planetary Defense Conference, Orange County, CA, AIAA Paper 2004-1447, Feb. 2004.

[14] Lu, E. T., and Love, S. G., "Gravitational Tractor for Towing Asteroids," *Nature*, Vol. 438, Nov. 2005, pp. 177–178. doi:10.1038/438177a

[15] Spitale, J. N., "Asteroid Hazard Mitigation using the Yarkovsky Effect," *Science*, Vol. 296, No. 5565, 2002, p. 77. doi:10.1126/science.1069577

[16] Melosh, H. J., Nemchinov, I. V., and Zetzer, Y. I., "Non-Nuclear Strategies for Deflecting Comets and Asteroids," *Hazard Due to Comets and Asteroids*, edited by T. Gehrels, Univ. of Arizona, Tucson, AZ, 1994, pp. 1110–1131.

[17] Olds, J., Charania, A., and Schaffer, M. G., "Multiple Mass Drivers as an Option for Asteroid Deflection Missions," 2007 Planetary Defense Conference, Washington, D.C., Paper 2007 S3-7, Mar. 2007.

[18] Schaub, H., and Junkins, J. L., *Analytical Mechanics of Space Systems*, AIAA Education Series, AIAA, Reston, VA, 2003, pp. 592–623.

[19] Battin, R. H., *Introduction to the Mathematics and Methods of Astrodynamics*, AIAA Education Series, AIAA, Reston, VA, 1999, pp. 484–490.

[20] Vasile, M., and Colombo, C., "Optimal Impact Strategies for Asteroid Deflection," *Journal of Guidance, Control, and Dynamics*, Vol. 31, No. 4, 2008, pp. 858–873.doi:10.2514/1.33432

[21] Sagan, C., *Pale Blue Dot: A Vision of the Human Future in Space*, Random House, Toronto, 1994, pp. 149–150.

[22] Hammerling, P., and Remo, J. L., "NEO Interaction with Nuclear Radiation," *Acta Astronautica*, Vol. 36, No. 6, 1995, pp. 337–346. doi:10.1016/0094-5765(95)00111-5

[23] Glasstone, S. (ed.), *The Effects of Nuclear Weapons*, Atomic Energy Commission, Washington, D.C., 1962.

[24] Wang, J., Davis, A. M., Clayton, R. N., and Hashimoto, A., "Evaporation of Single Crystal Forsterite: Evaporation Kinetics, Magnesium Isotope Fractionation, and Implications of Mass-Dependent Isotopic Fractional of a Diffusion-Controlled Reservoir,"

Geochimica et Cosmochimica Acta, Vol. 63, No. 6, 1999, pp. 953–966. doi:10.1016/S0016-7037(98)00286-5

[25] Holsapple, K. A., "The Scaling of Impact Processes in Planetary Science," *Annual Review of Earth and Planetary Sciences*, Vol. 21, May 1993, pp. 333–373. doi:10.1146/annurev.ea.21.050193.002001

[26] Scheeres, D. J., "Close Proximity Operations for Implementing Mitigation Strategies," AIAA Planetary Defense Conference, Orange County, CA, AIAA Paper 2004-1445, Feb. 2004.

[27] Wertz, J. R., and Larson, W. J., *Space Mission Analysis and Design*, 3rd ed., Microcosm, Torrance, CA, 2003, p. 703.

[28] Olds, J., Charania, A., Graham, M., and Wallace, J., "The League of Extraordinary Machines: A Rapid and Scalable Approach to Planetary Defense Against Asteroid Impactors," Vol. 1, NASA Inst. for Advanced Concepts, CP-NIAC 02-02, Atlanta, Apr. 2004.

[29] Lehmann, P., Reck, B., Behrens, J., and Vo, M. D., "Acceleration of a Suborbital Payload Using an Electromagnetic Railgun," *IEEE Transactions on Magnetics*, Vol. 43, No. 1, 2007, pp. 480–485. doi:10.1109/TMAG.2006.887666

[30] Ahrens, T. J., and Harris, A. W., "Deflection and Fragmentation of Near-Earth Asteroids," *Nature*, Vol. 360, Dec. 1992, pp. 429–433. doi:10.1038/360429a0

[31] Anttila, M., and Ylikorpi, T., "Defining the Technical Requirements for Subsurface Mars Driller," *Sixth International Conference on Mars*, Pasadena, CA, Luna Planetary Inst. Paper 3020, July 2003.

[32] Liu, Y., Weinberg, B., and Mavroidis, C., "Mechanical Design and Modelling of a Robotic Planetary Drilling System," 2006 International Design Engineering Technical Conferences, Philadelphia, American Society of Mechanical Engineers Paper DETC2006-99699 Sept. 2006.

[33] Thomas, M., "Inflatable Space Structures," *IEEE Potentials*, Vol. 11, No. 4, 1992, pp. 29–32.doi:10.1109/45.207143

[34] Hedgepeth, J. M., and Miller, R. K., "Structural Concepts for Large Solar Concentrators," *Acta Astronautica*, Vol. 17, No. 1, 1988, pp. 79–89. doi:10.1016/0094-5765(88)90131-2

[35] Harris, A. W., "The Rotation Rates of Very Small Asteroids: Evidence for 'Rubble Pile' Structure," *Lunar and Planetary Science*, Vol. 27, Mar. 1996, p. 493.

[36] Maddock, C., Sanchez, J. P., Vasile, M., and Radice, G., "Comparison of Single and Multi-Spacecraft Configurations for NEA Deflection by Solar Sublimation," *New Trends in Astrodynamics and Applications*, Vol. 886, American Inst. of Physics, Melville, NY, 2007, pp. 303–316.

[37] Vasile, M., "A Multi-Mirror Solution for the Deflection of Dangerous NEOs," *Journal of Communications in Nonlinear Science and Numerical Simulation* (to be published). doi:10.1016/j.cnsns.2008.09.005

[38] McInnes, C., "Near Earth Object Orbit Modification Using Gravitational Coupling," *Journal of Guidance, Control, and Dynamics*, Vol. 30, No. 3, 2007, pp. 870–873. doi:10.2514/1.25864

[39] Broschart, S. B., and Scheeres, D. J., "Control of Hovering Spacecraft Near Small Bodies: Application to Asteroid 25143 Itokawa," *Journal of Guidance, Control, and Dynamics*, Vol. 28, No. 2, 2005, pp. 343–354. doi:10.2514/1.3890

[40] Kawaguchi, J., Fujiwara, A., and Uesugi, T., "Hayabusa—Its Technology and Science Accomplishment Summary and Hayabusa-2," *Acta Astronautica*, Vol. 62, Nos. 10–11, 2008, pp. 639–647. doi:10.1016/j.actaastro.2008.01.028

[41] Vasile, M., "Robust Mission Design Through Evidence Theory and Multi-Agent Collaborative Search," *Annals of the New York Academy of Sciences*, Vol. 1065, 2005, pp. 152–173. doi:10.1196/annals.1370.024

[42] Vasile, M., "A Hybrid Multi-Agent Collaborative Search Applied to the Solution of Space Mission Design Problems," *International Workshop on Global Optimization (GO '05)*, Univ. of Almeria, Almeria, Spain, Sept. 2005, pp. 247–252.

[43] Valsecchi, G. B., "Close Encounters and Collisions of Near-Earth Asteroids with the Earth," *Comptes Rendus Physique*, Vol. 6, No. 3, 2005, pp. 337–344. doi:10.1016/j.crhy.2004.12.014

[44] De Pascale, P., and Vasile, M., "Preliminary Design of Low-Thrust Multiple Gravity Assist Trajectories," *Journal of Spacecraft and Rockets*, Vol. 43, No. 5, 2006, pp. 1065–1076. doi:10.2514/1.19646

[45] Mankins, J. C., "Approaches to Strategic Research and Technology (R&T) Analysis and Road Mapping," *Acta Astronautica*, Vol. 51, Nos. 1–9, 2002, pp. 3–21. doi:10.1016/S0094-5765(02)00083-8

[46] Moorhouse, D. J., "Detailed Definitions and Guidance for Application of Technology Readiness Levels," *Journal of Aircraft*, Vol. 39, No. 1, 2002, pp. 190–192. doi:10.2514/2.2916

[47] Ferri, P., and Schwehm, G., "Rosetta: ESA's Comet Chaser Already Making Its Mark," *ESA Bulletin*, Vol. 123, Aug. 2005, pp. 62–66.

[48] Blacic, J., Dreesen, D., and Mockler, T., "Report on Conceptual System Analysis of Drilling Systems for 200-m-Depth Penetration and Sampling of the Martian Subsurface," Los Alamos National Lab., TR LAUR00-4742, Los Alamos, NM, Oct. 2000.

[49] Basso, B., Bartlett, P., Gorevan, S., Kennedy, T., Paulsen, G., Wilson, J., and Yachbes, I., "Surface Anchoring and Deflection Concepts for Earth-crossing Comets and Asteroids," Workshop on Spacecraft Reconnaissance of Asteroid and Comet Interiors, Santa Cruz, CA, Luna Planetary Inst. Paper 3032, Oct. 2006.

[50] Vorontsov, M. A., Kolosov, V. V., and Kohnle, A., "Adaptive Laser Beam Projection on an Extended Target: Phase- and Field-Conjugate Precompensation," *Journal of the Optical Society of America*, Vol. 24, No. 7, 2007, pp. 1975–1993. doi:10.1364/JOSAA.24.001975

[51] Angel, R., Burge, J., Hege, K., Kenworthy, M., and Woolf, N., "Stretched Membrane with Electrostatic Curvature (SMEC): A New Technology for Ultra-Lightweight Space Telescopes," *UV, Optical and IR Space Telescopes and Instruments*, Vol. 4013, Society of Photo-Optical Instrumentation Engineers, Bellingham, WA, 2000, pp. 699–705.

[52] Composite Ultra-Light Weight Active Mirror for Space Applications, U.S. Patent 7064885, issued 10 Apr. 2005.

[53] "A New Deployable Thin-film, Ultralight Mirror for Future Space Telescopes and Surveillance Satellites," *Current Science*, Vol. 79, No. 1, 2000, p. 12.